PCMDI Report No. 56

Dynamical Seasonal Predictability of the Asian Summer Monsoon

by

K. R. Sperber[1], C. Brankovic[2], M. Déqué[3], C. S. Frederiksen[4] , R. Graham[5] , A. Kitoh[6] , C. Kobayashi[7] , T. Palmer[2] , K. Puri[4] , W. Tennant[8] , and E. Volodin[9]

1 Program for Climate Model Diagnosis and Intercomparison, Lawrence Livermore National Laboratory, Livermore, CA USA
2 European Centre for Medium-Range Weather Forecasts, Reading, United Kingdom
3 Centre National de Recherches Météorologiques, Toulouse, France
4 Bureau of Meteorology Research Centre, Melbourne, Australia
5 United Kingdom Meteorological Office, Bracknell, United Kingdom
6 Climate Research Department, Meteorological Research Institute, Japan Meteorological Agency, Tsukuba, Japan
7 Climate Prediction Division, Japan Meteorological Agency, Tokyo, Japan
8 South African Weather Bureau, Pretoria, South Africa
9 Department of Numerical Mathematics, Moscow, Russia

July 2000

**PROGRAM FOR CLIMATE MODEL DIAGNOSIS AND INTERCOMPARISON
UNIVERSITY OF CALIFORNIA, LAWRENCE LIVERMORE NATIONAL
LABORATORY, LIVERMORE, CA 94550**

DISCLAIMER

Dynamical Seasonal Predictability of the Asian Summer Monsoon

K. R. Sperber[1], C. Branković [2], M. Déqué[3],
C. S. Frederiksen[4], R. Graham[5], A. Kitoh[6],
C. Kobayashi[7], T. Palmer[2], K. Puri[4],
W. Tennant[8], and E. Volodin[9]

[1]Program for Climate Model Diagnosis and Intercomparison, Lawrence Livermore National Laboratory, Livermore, CA USA

[2]European Centre for Medium-Range Weather Forecasts, Reading, United Kingdom

[3]Centre National de Recherches Météorologiques, Toulouse, France

[4]Bureau of Meteorology Research Centre, Melbourne, Australia

[5]United Kingdom Meteorological Office, Bracknell, United Kingdom

[6]Climate Research Department, Meteorological Research Institute, Japan Meteorological Agency, Tsukuba, Japan

[7]Climate Prediction Division, Japan Meteorological Agency, Tokyo, Japan

[8]South African Weather Bureau, Pretoria, South Africa

[9]Department of Numerical Mathematics, Moscow, Russia

Corresponding Author:
Dr. Kenneth R. Sperber
Program for Climate Model Diagnosis and Intercomparison
Lawrence Livermore National Laboratory
P.O. Box 808, L-264
Livermore, CA 94550 USA

Ph: (925) 422-7720
Fax: (925) 422-7675
Email: sperber@space.llnl.gov

ABSTRACT

Ensembles of hindcasts from seven models are analyzed to evaluate dynamical seasonal predictability of the Asian summer monsoon (ASM) during 1987, 1988, and 1993. These integrations were performed using observed sea surface temperatures and from observed initial conditions. The experiments were performed at the behest of the CLIVAR Working Group on Seasonal to Interannual Prediction as part of the Seasonal prediction Model Intercomparison Project (SMIP). Integrations from the European Union PROVOST (PRediction of climate Variations on Seasonal to interannual Timescales) experiment are also evaluated.

The National Centers for Environmental Prediction/National Center for Atmospheric Research and European Centre for Medium-Range Weather Forecasts reanalyses and observed pentad rainfall form the baseline against which predictability is judged. The time-mean state and the interannual and subseasonal variability are evaluated. It is demonstrated that to varying degree the models can simulate the hierarchy of modes that are important for controlling the subseasonal variability of the 850hPa flow during the ASM. In many cases the models represent the strong link between the 850hPa flow and rainfall observed on subseasonal timescales. However, deficiencies in the simulation of the subseasonal modes contribute directly to poor seasonal predictability and are related to systematic error of the mean state. With regard to dynamical seasonal predictability, in most instances the models fail to properly project the subseasonal modes onto the interannual variability with result that hindcasts of ASM are poor. In cases where the observed modes are known to be related to the boundary forcing, the failure of the models to properly project the modes onto the interannual variability indicates that the models are not setting up observed teleconnection patterns.

1. Introduction

The roots of contemporary seasonal forecasting of the boreal summer monsoon, in particular the Indian monsoon, date back to the late 1870's/early 1880's (Normand, 1953). H. F. Blanford, the father of the All-India Meteorological Service, based his forecasts of Indian monsoon rainfall on preseason snowcover in the Himalayas (Blanford 1884). Presently, the role of Himalayan (and Eurasian) snowcover as a precursor to monsoon rainfall is still the subject of much debate and investigation (Barnett et al. 1989, Ferranti and Molteni 1999, Becker et al. 2000). In the 1920's/1930's, Sir Gilbert Walker imposed mathematical rigor to the forecast problem, introducing the use of the correlation coefficient to the meteorological community, with the goal of determining the conditions that "foreshadow" Indian summer monsoon rainfall (Walker and Bliss 1930). To this day, seasonal forecasts of summer monsoon rainfall are based primarily on statistical methods that take into account key indices that are typically associated with slowly varying components of the climate system, such as the El Niño/Southern Oscillation (ENSO; Krishna Kumar et al. 1995).

Dynamical seasonal predictability, if successful, would provide advantages over statistical methods, including (but not limited to): (1) a reliable estimate of the magnitude and regionality of the rainfall anomalies, and (2) the estimate of confidence bounds of the forecast based upon the spread of the ensemble members. However, dynamical seasonal predictability of the Asian summer monsoon (ASM) has remained elusive, as illustrated by the lack of predictability exhibited by integrations performed under the European Union PROVOST (Prediction of Climate Variations on Seasonal to Interannual Timescales) project (Brankovic and Palmer 2000). In this case, a contributing factor to the poor predictability was the magnitude of the systematic error of the seasonal mean monsoon, with the largest errors occurring in the vicinity of the tropical convergence zones (TCZ). These errors were of a magnitude comparable to the signal that was to be predicted. Furthermore, Sperber and Palmer (1996) have shown that the teleconnection between all-India rainfall and tropical sea surface temperature (SST) is not captured well by general circulation models (GCMs). Predictability may also be limited by an additional complicating factor, namely the projection of chaotic subseasonal variability onto the seasonal mean. For example, Krishnamurti and Bhalme (1976), Sikka (1980), and Gadgil and Asha (1992) find that years of below-normal all-India rainfall (AIR) tend to be characterized by prolonged monsoon breaks with the TCZ preferentially located over the Indian Ocean. The degree to which the subseasonal modes are chaotic will have a direct impact on the predictability of the system.

Until recently, the main body of evidence supporting a link between subseasonal and interannual variability was based upon model simulations (Fennessy and Shukla 1994, Ferranti et al. 1997), mainly through circumstantial evidence based upon the similarity of the spatial patterns of subseasonal and interannual variability. This similarity led Palmer (1994) to propose a paradigm in which intraseasonal variability is essentially chaotic, with the interannual variability being governed by the frequency of occurrence of the active (continental) versus the break (oceanic) regimes. Consistent with the ideas of Charney and Shukla (1981), the suggestion is that the boundary forcing (e.g., SST) biases the system towards more active or break regimes.

With the long record afforded by the National Centers for Environmental Prediction/National Center for Atmospheric Research (NCEP/NCAR) reanalysis (Kalnay et al. 1996), Sperber et al. (1999, 2000) investigated the link between subseasonal and interannual variability during the Asian summer monsoon for the period 1958-97. Using daily 850hPa winds over the ASM region, they revealed a subset of the subseasonal modes of variability that a model must simulate in order to yield the potential for seasonal predictability of the ASM. They identified a hierarchy of subseasonal modes associated with the northward propagation of the TCZ, and a common mode of variability that controlled the subseasonal and interannual variations of rainfall over India. Additionally, they clearly demonstrated that low-frequency variations of the basic state were responsible for systematically perturbing a subset of these modes, thus yielding the potential for probabilistic predictability of some aspects of the ASM.

The goals of this paper are to investigate ensembles of hindcasts of the ASM to determine: (1) Can GCMs accurately simulate the hierarchy of modes that are important for controlling the subseasonal variability of the ASM? (2) Can the models represent the strong link between the 850hPa flow and the rainfall found on subseasonal timescales? (3) If so, are these modes correctly projected onto the seasonal mean monsoon to produce observed interannual variations? (4) Is it possible to objectively discriminate among the ensemble members to ascertain which members are most reliable? Additionally, the results are also of benefit since they highlight the modes that most contribute to errors of the mean states of the individual models.

The experimental design and the participating models are discussed in Section 2. The time-mean state of the models are presented in Section 3, and in Section 4 the subseasonal modes are evaluated. In Section 5 the projections of the subseasonal modes onto the interannual variability are presented, and discussions and conclusions are given in Section 6.

2. The Experimental design, the models, and data

Over the past several years, various efforts to assess dynamical seasonal predictability (DSP) have been undertaken. The most ambitious effort in this regard was the European Union PROVOST Project. This project consisted of ensembles of seasonal length (approximately 120 days) integrations for each season for the period 1979-93, the period covered by the European Centre for Medium-Range Weather Forecasts (ECMWF) Reanalysis (Gibson et al. 1996, 1997). Given the scope of this project only a limited number of modelling groups had the resources necessary to participate, and the project was European based. In an effort to assess DSP in a wider range of models, the Climate Variability and Predictability (CLIVAR) Numerical Experimentation Group-1 (now the Working Group on Seasonal to Interannual Predictability) initiated the Seasonal Prediction Model Intercomparison Project (SMIP) at the suggestion of Dr. J. Shukla (Center for Ocean-Land-Atmosphere Studies). In all cases the models were forced with observed SST's, and the initial conditions were taken from ECMWF Reanalysis (in the case of PROVOST) or optionally NCEP/NCAR Reanalysis in the case of SMIP.

The integrations analyzed in this paper consist of those simulations that were contributed to the DSP archive at the Program for Climate Model Diagnosis and Intercomparison (PCMDI), and for which there were common years for which hindcasts were made. Thus, we analyze summer monsoon hindcasts for 1987, 1988, and 1993. These years correspond to El Niño, La Niña, and near-normal conditions in the tropical Pacific Ocean, respectively. For these years we evaluate daily 850hPa winds and rainfall for the period 1 June-30 September. The models employed, and some of their basic characteristics are presented in Table 1. The models span a wide-range of horizontal and vertical resolutions, with the contribution from the South African Weather Bureau (SAWB) having the coarsest resolution, while the ECMWF model has the highest resolution. Further details of the formulations of the various models can be found in the references given in Table 1.

The daily 850hPa wind from the NCEP/NCAR Reanalysis is used to characterize the subseasonal and interannual variability over the ASM region. The reanalysis is a joint project between NCEP and NCAR to produce a multi-decadal record of global atmospheric analyses with a data assimilation system that is unchanged (Kalnay et al. 1996). The data assimilation and forecast model are based on the global system that was implemented operationally at NCEP in January 1995. The model is run at a horizontal resolution of T62 and with 28 vertical levels. Moist convection is represented by a simplified form of the Arakawa-Schubert parametrization scheme (Pan

Table 1: Model Attributes.

Model	Resolution	Version	No. of Runs	References
BMRC (Australia) Bureau of Meteorology Research Centre	R31 L17	3.7	4	Hart et al. (1990) McAvaney and Coleman (1993)
CNRM (France) Centre National de Recherches Météorologiques	T42 L31	Arpege/IFS Cycle 12	5	Déqué and Piedelievre (1995)
DNM (Russia) Department of Numerical Mathematics	4°x5^{o} L21	A5421	4	Alekseev et al. (1999)
ECMWF (England) European Centre for Medium-Range Weather Forecasts	T63 L31	Cycle 13R4	9	Miller et al (1995) Gibson et al. (1997)
JMA (Japan) Japan Meteorological Agency	T63 L30	GSM9603	4	JMA (1997)
SAWB (South Africa) South African Weather Bureau	T30 L18	COLA Version 1	4	Kirtman et al. (1997) Tennant (1999)
UKMO (England) United Kingdom Meteorological Office	2.5^{o}x3.75^{o} L19	HadAM2b	4	Hall et al. (1995) Graham et al. (2000)

and Wu 1994) and clouds are diagnosed from model variables using a scheme based on Slingo (1987). The NCEP model uses a 3-layer soil scheme based on that of Pan and Mahrt (1987) in which the temperature of the bottom layer is set to the annual mean climatological value. Data were assimilated using a spectral statistical interpolation/3-D variational analysis method which requires no nonlinear normal-mode initialization. Monthly mean upper air data on standard pressure surfaces have been supplied, already gridded onto a 2.5˚ latitude/longitude grid. Surface and 24 hour forecast fields (e.g., precipitation) are given on the equivalent T62 Gaussian grid. The spin-up of the hydrological cycle is small in the NCEP/NCAR reanalysis (e.g. Mo and Higgins 1996; Stendel and Arpe 1997).

The subseasonal variations of rainfall are determined using the Climate Prediction Center Merged Analysis of Precipitation (CMAP). This data set uses essentially the same algorithm and data sources as the monthly CMAP dataset described by Xie and Arkin (1997). The version we use is based on a blend of gauge data with satellite products, including GPI (GOES Precipitation Index based on geostationary infrared data), MSU (Microwave Sounding Unit), OPI (Outgoing longwave radiation-based Precipitation Index), SSM/I (Special Sensor Microwave/Imager) scattering and SSM/I emission. A detailed description of the pentad CMAP data set is in preparation (Pingping Xie, personal communication 1999).

To provide evidence of the robust nature of the subseasonal variations of the 850hPa winds we have also analyzed the European Centre for Medium-Range Weather Forecasts Reanalysis (ERA). A full description of the ERA is available in Gibson et al. (1996, 1997). It was performed using a special version of the ECMWF operational data assimilation system which includes a spectral T106 forecast model with 31 hybrid vertical levels and a fully three dimensional semi-Lagrangian advection scheme. The forecast model is based on version 13r4 of the ECMWF Integrated Forecast System (IFS) which was used operationally between April 1995 and January 1996. In particular, the parametrization of moist processes uses the convective mass flux scheme of Tiedtke (1989) with prognostic clouds (Tiedtke 1993). The land surface scheme of Viterbo and Beljaars (1995) is employed which is based on a 4-layer soil model and includes the effects of vegetation. A zero heat flux lower boundary condition is imposed and thus deep soil temperatures are not constrained to any climatology. Analyses were created every 6 hours and a diabatic, non-linear normal mode initialization was applied. The 6-hourly T106 spectral upper air data on model levels have been post-processed to provide a range of variables on standard pressure levels at 2.5^{o}x2.5^o resolution.
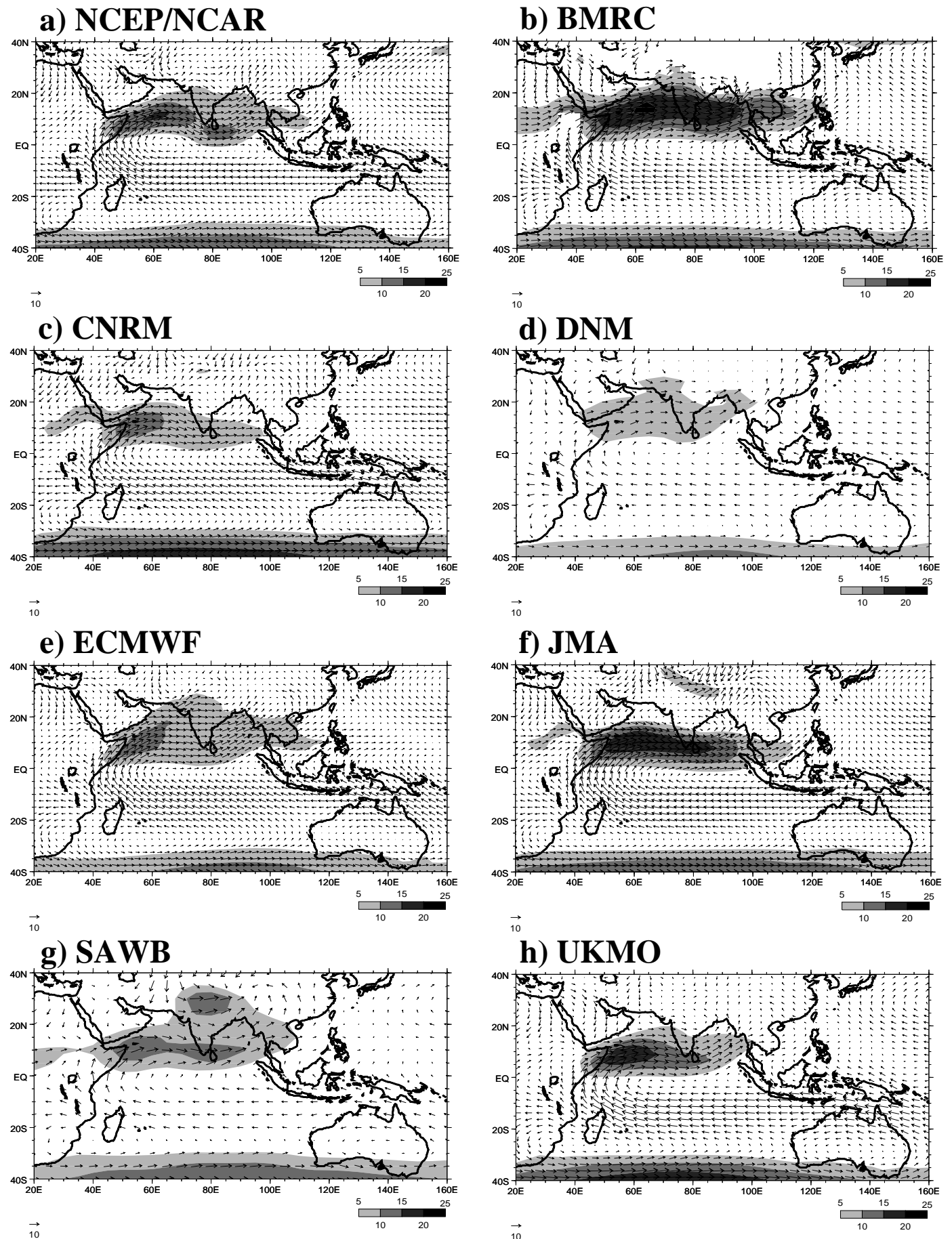
Figure 1: Time-mean 850hPa wind for June-September 1987, 1988, and 1993. The zonal wind is shaded where it is $\geq$5m s^{-1}. A unit vector corresponds to 10m s^{-1}.

a) Xie-Arkin

b) BMRC

c) CNRM

d) DNM

e) ECMWF

f) JMA

g) SAWB

h) UKMO
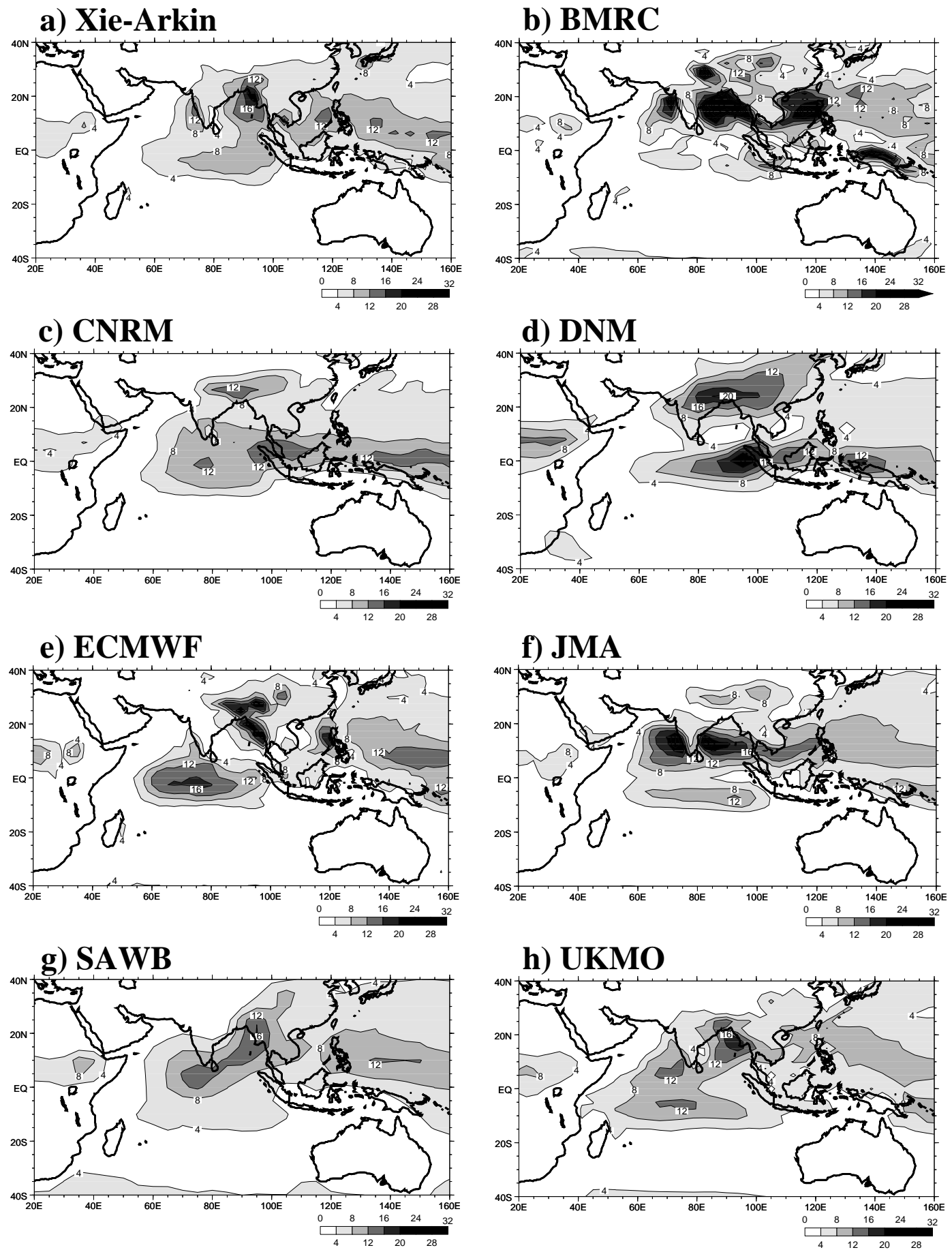
Figure 2: Time-mean rainfall for June-September 1987, 1988, and 1993. Contours and shading are plotted at 4, 8, 12,... mm day^{-1}.

-7-

3. Time-mean of the 850hPa wind and rainfall

The lower tropospheric Somali Jet is one of the most dramatic elements of the the Asian summer monsoon. Initially, it develops in response to the land/sea temperature contrast due to the seasonal change in solar heating. Subsequently, the latent heating associated with convection plays an increasingly important role in the maintenance of the Somali Jet as the monsoon season progresses. Importantly, the 850hPa flow captures important elements of the large-scale and regional-scale monsoon circulation on interannual and subseasonal timescales (Webster et al. 1998, Annamalai et al. 1999, Sperber et al. 2000).

The time-mean of the June-September 850hPa wind from the NCEP/NCAR reanalysis and the models for 1987, 1988, and 1993 are given in Fig. 1. While this is a short record, the spatial pattern of the reanalysis climatology in Fig. 1a is robust with respect to its climatology for 1958-97 presented in Sperber et al. (2000a). However, in the more restricted record presented here the flow over central India and the western Bay of Bengal is slightly more zonal, and the monsoon circulation is weaker by 1-2 ms^{-1} (not shown). This is consistent with the interdecadal variability of the monsoon circulation discussed in Sperber et al. (2000a). The time-mean of the ensembles from each model show a wide-variety of 850hPa flow patterns. CNRM, DNM, ECMWF, and SAWB (Figs. 1c, d, e, and g) underestimate the strength of the Somali Jet, especially over the Arabian Sea. BMRC and JMA (Figs. 1b and f) overestimate the strength of the jet. Additionally, in BMRC the core of the jet penetrates directly across India, rather than showing evidence of recurvature to the south as in the reanalysis (Fig. 3a). Additionally, there is pronounced cyclonic activity at the head of the Bay of Bengal which not evident in the reanalysis. In UKMO (Fig. 1h) the jet is too strong over the Arabian Sea and too weak over East Asia. In CNRM, JMA and UKMO (Figs. 1c, f, and h) the jet does not extend far enough northward, being too weak over northern India and the Bay of Bengal. In SAWB (Fig. 1g), the westerlies are too strong over northern India, with this component of the flow being dominated by dry air advection from the Thar desert. The differences between the time-mean states of the models and the reanalysis are larger than the difference between the reanalysis for the restricted record versus the 1958-97 record, and the difference between the NCEP/NCAR and ERA reanalyses presented in Annamalai et al. (1999). This indicates that substantial errors exist in the simulations of the low-level summer monsoon circulation.

The time-mean precipitation from the observations and models are presented in Fig. 2. The time-mean of the Xie and Arkin (1996) observed rainfall for 1987, 1988, 1993 is extremely robust (Fig. 2a), being virtually identical to that for the period 1979-

95 shown in Annamalai et al. (1999). The errors in the simulated time-mean rainfall typically reflect the errors in the 850hPa flow. This is consistent with the flow in the tropics being governed mainly by the diabatic heating. BMRC and JMA (Figs. 2b and f) tend to overestimate the rainfall in their TCZ's. In BMRC the overly strong rainfall at the head of the Bay of Bengal is consistent with this models incorrect simulation of cyclonic activity there. For JMA (Fig. 2f), the rainfall at the head of the Bay of Bengal is underestimated in association with the weak low-level flow in that region (Fig. 1f). For CNRM, DNM, ECMWF, and UKMO (Figs. 2c, d, e, and h) the enhanced rainfall along the west coast of India is poorly represented in association with the Somali jet being too weak and/or not extending far enough to the north. For the ECMWF model, the dry bias over Indian has been a pervasive problem, dating back to earlier versions of the model (Sperber et al. 1994). As noted above, SAWB has substantial dry air advection from the Thar desert, consistent with the underestimate of rainfall over northern India (Fig. 2g).

In many cases the systematic error of the simulated rainfall and the 850hPa wind are substantial. This suggests that many of the models many be of limited usefulness for seasonal predictability of the ASM. The degree to which this is the case, and the relation between errors in the climatologies and errors in the simulation of subseasonal variability will be explored in subsequent sections of the paper.

4. Subseasonal variability

a) EOF analysis of the 850hPa flow

Subseasonal variability is characterized via empirical orthogonal function (EOF) analysis of the 850hPa winds, as performed in Sperber et al. (2000). Prior to the analysis the climatological daily means (over all members of an individual models ensembles in the case of the hindcasts) have been removed at each gridpoint. EOF analysis of the NCEP/NCAR reanalyzed winds for 1987, 1988 and 1993 reveals that EOF's 1-3 (Figs. 3a, 4a, and 5a) are very robust, being virtually identical to their counterparts extracted from the 40 years of reanalysis examined by Sperber et al. (2000). Additionally, these modes are consistent with those from the ERA data for 1987, 1988, and 1993 (not shown). The correlations of the NCEP/NCAR principal components (PC's) with their counterparts from ERA are 0.99, 0.95 and 0.88 respectively. These results attest to the importance of these modes for controlling the subseasonal variability over the ASM region.

EOF's 1-2 are associated with the northward propagation of the TCZ, while EOF-3 is a common mode of variability that is most important for controlling subseasonal
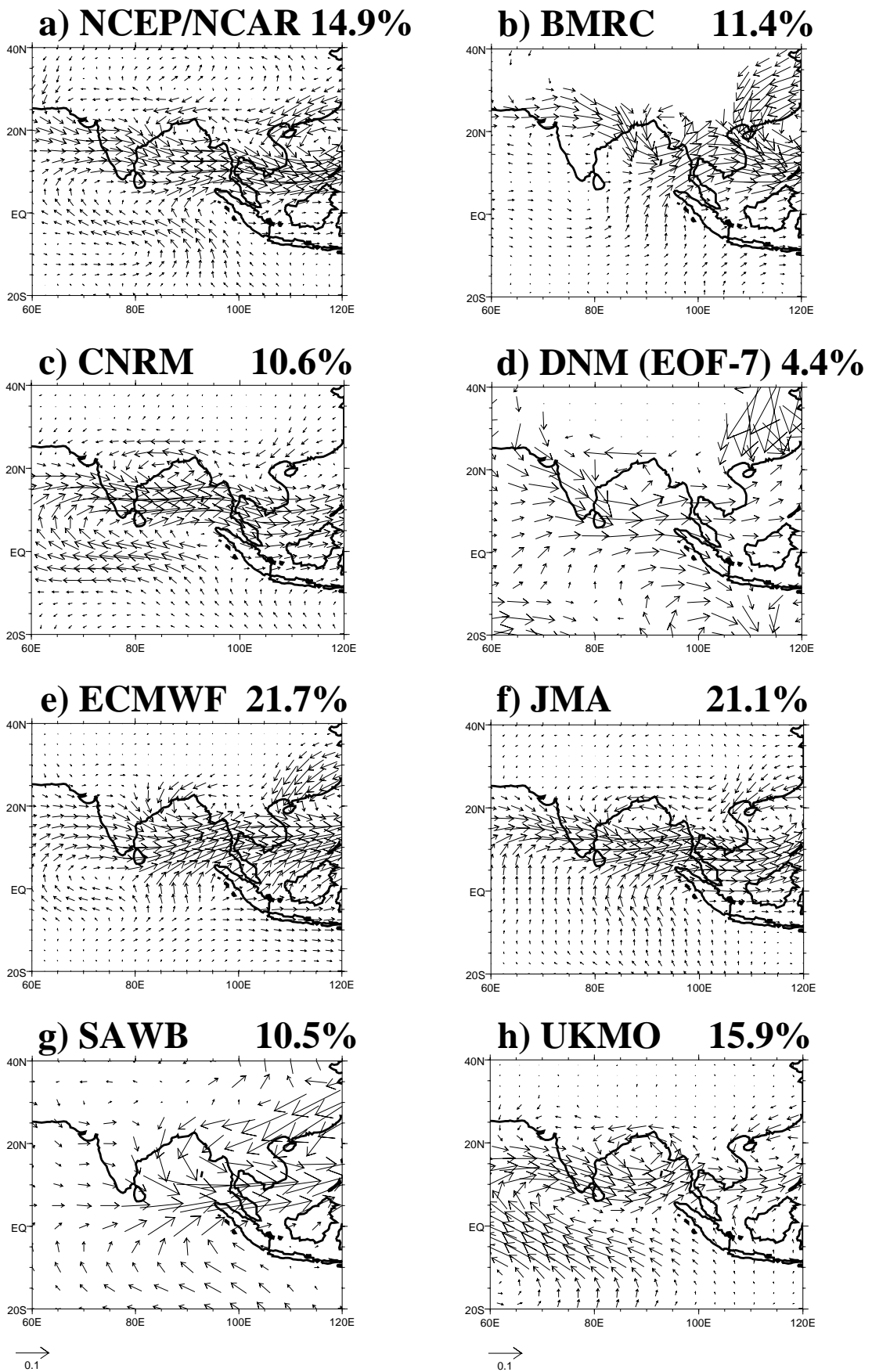
Figure 3: EOF-1 of daily 850hPa wind anomalies (calculated with respect to the climatological daily means) for June-September 1987, 1988, and 1993. The percentage variance explained is also given.

and interannual variations of rainfall over India (Sperber et al. 2000). Given the robustness of the reanalyzed modes we have therefore decided to perform the EOF analysis separately for each model (using all ensemble members) rather than performing a common principal component analysis of all models jointly. Additionally, a single analysis over all models would be a substantial compromise given the wide range of model performance in simulating the climatologies of the rainfall and 850hPa flow. Identification of the model modes as counterparts to the observed modes requires that the spatial patterns of the EOF's and their influence on subseasonal rainfall both be qualitatively consistent with observations.

As seen in Figs. 3c, e, f, and h, CNRM, ECMWF, JMA, and UKMO are very realistic in their representation of EOF-1 from the reanalysis (Fig. 3a), particularly over the Asian continental latitudes. In CNRM and UKMO (Figs. 3c and h) the cyclonic flow near the South China Sea tends to be too weak, while CNRM, JMA and UKMO (Figs. 3c, f, and h) exhibit discrepancies in the western/central equatorial/southern Indian Ocean. While this is a region where few observations were available to constrain the reanalyses, the model differences are larger than the differences between the reanalyses (not shown). In BMRC (Fig. 3b) the westerly anomalies over India are displaced too far to the north. EOF-7 of DNM (Fig. 3d) is the counterpart to observed EOF-1. This model fails to capture the well defined regionality of the westerly anomalies. SAWB (Fig. 3g) exhibits substantial departures from the observed mode, in particular the westward extension of the cyclonic flow into the Bay of Bengal. Additionally, in the case of ECMWF and JMA (BMRC, CNRM, DNM, and SAWB) this mode accounts for a larger (smaller) fraction of the total variability than is observed.

EOF-2 (Fig. 4) is complimentary to EOF-1, being associated with the initiation of the northward propagation of the TCZ (Sperber et al. 2000). Relative to EOF-1 (Fig. 3a) the westerlies are located south of the continental latitudes, and in the Bay of Bengal the cyclonic flow is also displaced further south (Fig. 4a). Over the continental regions easterly anomalies are present. ECMWF, JMA, and UKMO (Figs. 4e, f, and h) are most realistic in their representation of this mode although discrepancies east of 100^oE are apparent relative to the reanalysis. CNRM (Fig. 4c) captures the large-scale characteristics of this mode, but fails to simulate the regionality of the closed cyclonic flow in the Bay of Bengal. From BMRC (Fig. 4b), EOF-3 is the counterpart to EOF-2 from the reanalysis. In this model the westerly anomalies are displaced further south than in EOF-1, but they are still located over the Indian subcontinent contrary to the reanalysis. This is consistent with this models bias in the mean state based on the overly strong Somali Jet core penetrating over the subcontinent in the

a) NCEP/NCAR 8.8%

b) BMRC (EOF-3) 5.8%

c) CNRM 7.6%

d) DNM

e) ECMWF 5.8%

f) JMA 8.0%

g) SAWB 6.6%

h) UKMO 8.3%

0.1

0.1
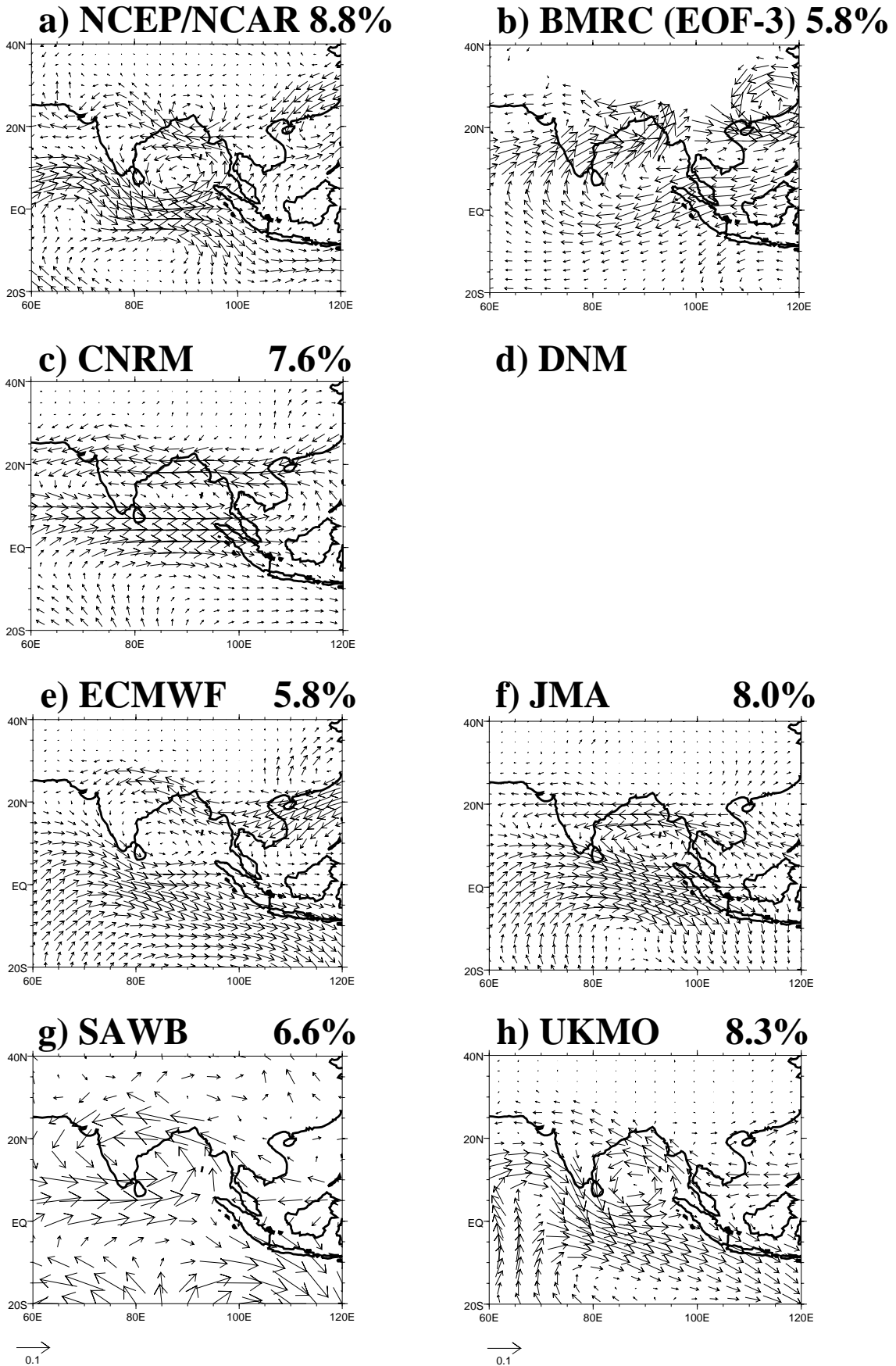
Figure 4: As Fig. 3 for EOF-2. DNM did not simulate a counterpart to observed EOF-2.

a) NCEP/NCAR 7.2%

b) BMRC (EOF-2) 7.7%

c) CNRM   5.8%

d) DNM (EOF-4) 7.2%

e) ECMWF   5.3%

f) JMA   7.4%

g) SAWB   6.2%

h) UKMO (EOF-4) 5.3%
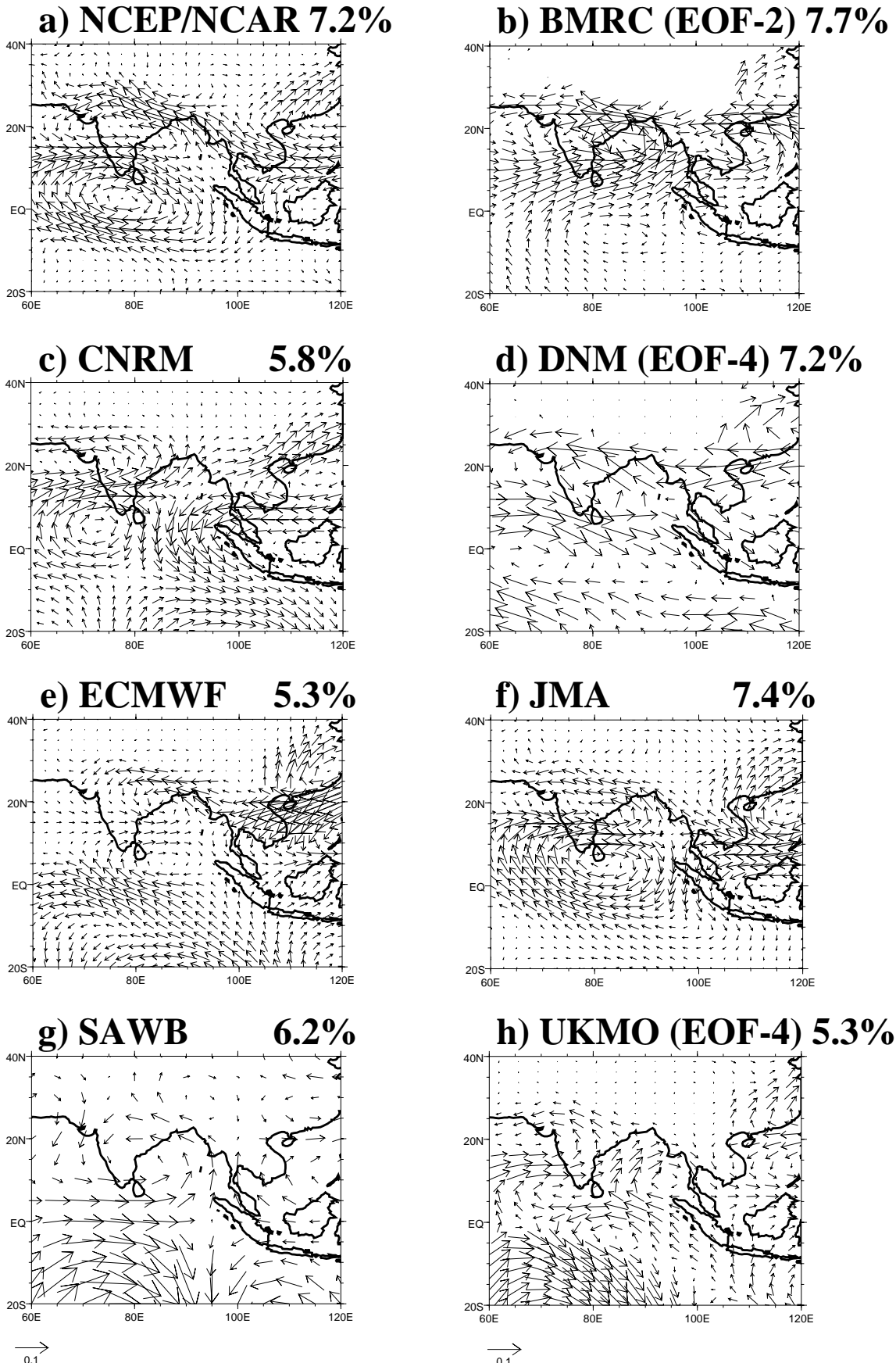
Figure 5: As Fig. 3 for EOF-3.

-13-

absence of southward recurvature of the flow (Fig. 1b). Additionally, the cyclonic flow in the Bay of Bengal is located too far to the north (also incorrectly present in EOF-2, this models counterpart to observed EOF-3, Fig. 5), which is consistent with the systematic error of this model to incorrectly produce cyclonic anomalies at this location in the mean state. SAWB (Fig. 4g) overestimates the cyclonic flow, placing it directly over the Indian subcontinent. All of the simulations poorly represent the observed flow over the South China Sea. DNM fails to capture a counterpart to the observed mode based on examination of the 10 EOF's retained in our analysis.

EOF-3 (Fig. 5) is the mode of major import for subseasonal and interannual variations of all-India rainfall (Sperber et al. 2000). This mode is characterized by a cyclonic/anticyclonic pattern over and to the south of the Indian subcontinent. Over East Asia anticyclonic anomalies prevail, while to the south near the Maritime continent the tendency is for cyclonic anomalies. JMA (Fig. 5f) is most adept at capturing this mode of variability seen in the reanalysis (Fig. 5a). CNRM and UKMO (EOF-4; Figs. 5c, h) exhibit a westward displacement of the cyclone/anticyclone pair in the vicinity of India, while BMRC (EOF-2) and ECMWF (Figs. 5b, e) have an eastward shift of this couplet relative to the reanalysis. DNM (EOF-4) and SAWB (Figs. 5d, g), the models with the coarsest horizontal resolution, are less realistic in their representation of this mode, failing to capture the strong gradients of the flow. With the exception of JMA the models poorly represent the regionality of the flow east of 100°E and south of the equator.

b) Relationship of the EOF's/PC's and rainfall

The rainfall anomalies associated with these modes of variability are given in Figs. 6-8. These are composite differences of rainfall for +/-1 standard deviation thresholds of the respective principal components (PC's). As mentioned earlier, EOF-1/PC-1 is associated with the tropical convergence zone. This is confirmed in Fig. 6a using the CMAP rainfall. Consistent with the 40-year analysis in Sperber et al. (2000), EOF-1/PC-1 is associated with a zonally oriented band of enhanced rainfall that extends from the Indian subcontinent to the western Pacific, with the largest loadings being located over the western Pacific. CNRM, JMA, and UKMO (Figs. 6c, f, and h), models with the most realistic representation of EOF-1 (Fig. 3), have good representations of the rainfall anomalies associated with EOF-1/PC-1. However, they tend to overestimate the rainfall anomalies over India and the Bay of Bengal. Additionally, in the case of CNRM (Fig. 6c), the positive rainfall anomalies over the South China Sea are too weak, consistent with the weaker than observed cyclonic flow there

a) CMAP

b) BMRC

c) CNRM

d) DNM (PC-7)

e) ECMWF

f) JMA

g) SAWB

h) UKMO
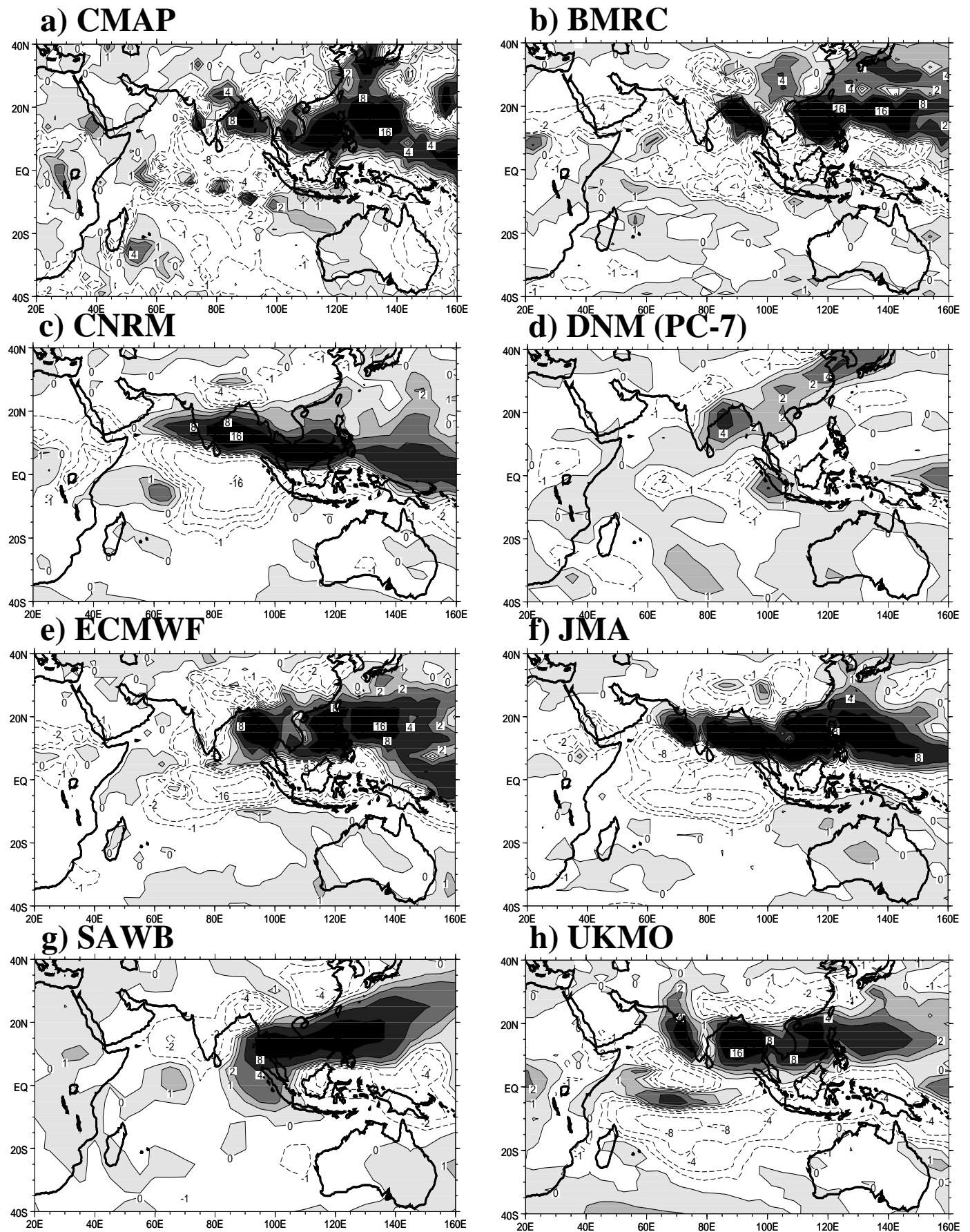
Figure 6: Difference of daily composites of rainfall based on strong-weak days of the principal component (PC) time series of EOF-1 using 1.0 and -1.0 standard deviation thresholds to define extreme days. The CMAP validation data is pentad based. The standardized daily PC time series was pentad averaged with extreme pentads defined using 1.0 and -1.0 standard deviation thresholds. Positive anomalies are shaded and the contour interval is +/-0, 1, 2, 4, 8,...mm day^{-1}.

(Fig. 3c). ECMWF (Fig. 6e), which also had an excellent EOF-1 pattern (Fig. 3e), captures the zonal band of enhanced rainfall from the Bay of Bengal to the western Pacific, but fails to capture the enhanced rainfall over India seen in the CMAP rainfall (Fig. 6a). This failure is consistent with the pronounced dry bias in the time-mean rainfall that this model exhibits over India (Fig. 2e). Similarly, the dry bias over India in SAWB (Fig. 2g) is consistent with the negative precipitation anomalies from the composite based on PC-1 (Fig. 6g), and the large underestimate of rainfall over India associated with PC-3 (Fig. 8g). Also, for SAWB recall that the basic structure of EOF-1 was different from the observed mode, such that the zonally oriented band of enhanced rainfall is associated with the improperly simulated westward extension of the cyclonic flow from the west Pacific to the Bay of Bengal. For BMRC, the rainfall associated with PC-1 (Fig. 6b) is also incorrect over India, but in the time-mean (Fig. 2b) this is compensated for by the projections of PC-3 (Fig. 7b) and PC-2 (Fig. 8b) in which the rainfall is grossly overestimated over this region. This indicates that the reasonably realistic rainfall climatology over India from this model (Fig. 2b) is obtained due to an unrealistic representation of the subseasonal rainfall variability. For DNM (Fig. 6d) the rainfall anomalies over India are too weak or of the wrong sign, the enhanced rainfall has a southwest to northeast tilt, consistent with the discrepancies of this mode (Fig. 3d), namely pronounced southwesterlies and convergence near southeast China.

The rainfall associated with EOF-2/PC-2 is given in Fig. 7. Relative to EOF-1, the positive rainfall anomalies (Fig. 7a) are weaker and displaced slightly southward, especially over the Bay of Bengal and southeast Asia. CNRM, ECMWF and JMA (Fig. 7c, e and f) are most realistic in representing the rainfall anomalies associated with the second mode. UKMO (Fig. 7h) performs best over India and the Bay of Bengal, but fails to capture the extension of enhanced rainfall to the South China Sea, precisely where this model exhibited errors in EOF-2 (Fig. 4h). Similarly, BMRC (EOF-3) and SAWB (Figs. 7b and g) exhibit substantial errors over the South China Sea.

For EOF-3/PC-3 the main signature in the observed rainfall (Fig. 8a) is the southeastward tilt of enhanced rainfall that extends from India to the Maritime continent. Over India the enhanced rainfall is associated with the cyclonic anomalies seen in Fig. 5a, while in the western Pacific 120°-140°E, 10°-25°N) and near the equator south of India the below-normal rainfall is associated with anticyclonic anomalies. The below-normal rainfall south of India is not as pronounced as from the longer record analyzed by Sperber et al. (2000). BMRC, CNRM, ECWMF, JMA and UKMO (Figs. 8b, c, e, f, and h) are most realistic in representing the rainfall anomalies in the

a) CMAP
b) BMRC (PC-3)
c) CNRM
d) DNM
e) ECMWF
f) JMA
g) SAWB
h) UKMO
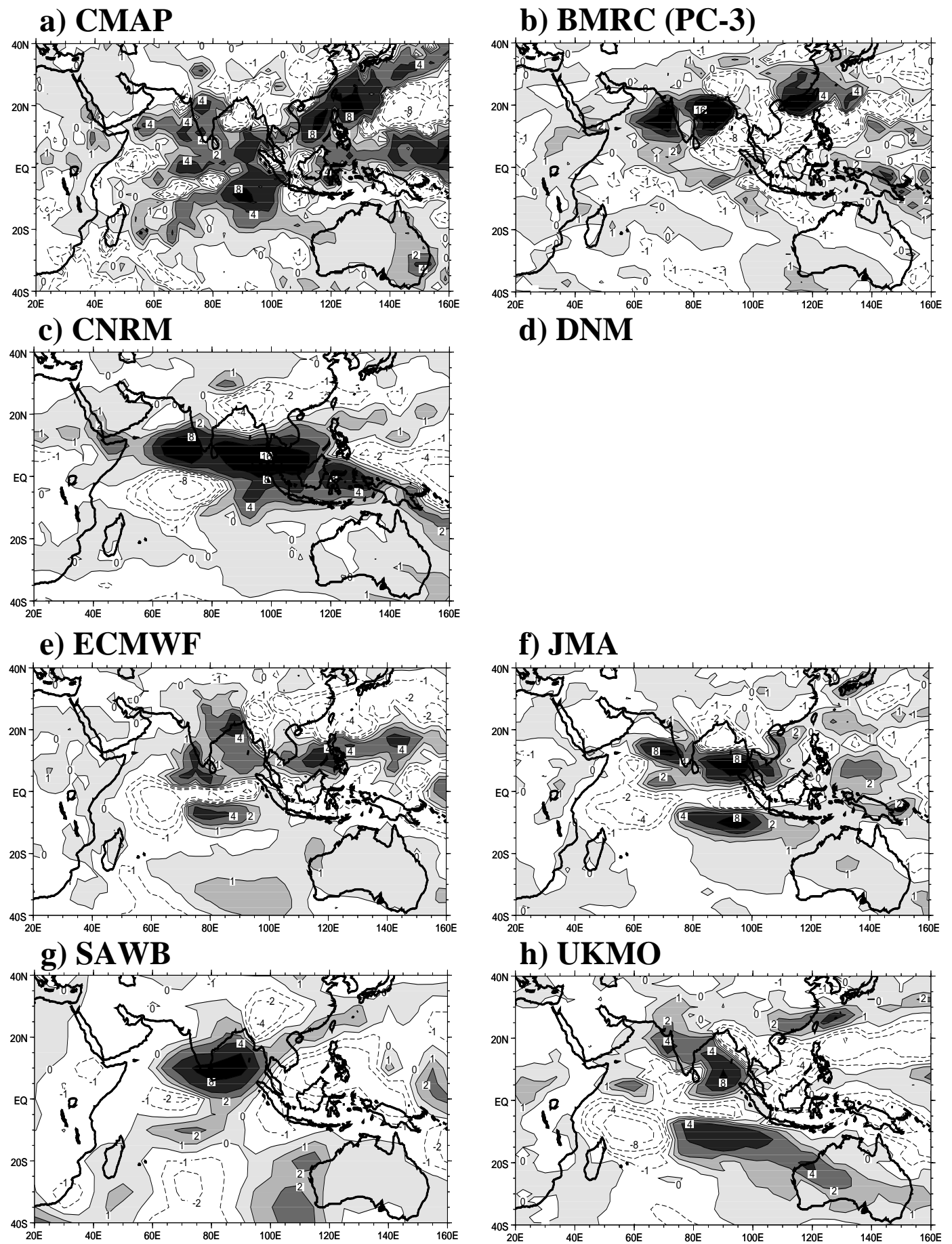
Figure 7: As Fig. 6 for EOF-2/PC-2.

-17-

a) CMAP

b) BMRC (PC-2)

c) CNRM

d) DNM (PC-4)

e) ECMWF

f) JMA

**g) SAWB**

h) UKMO (PC-4)
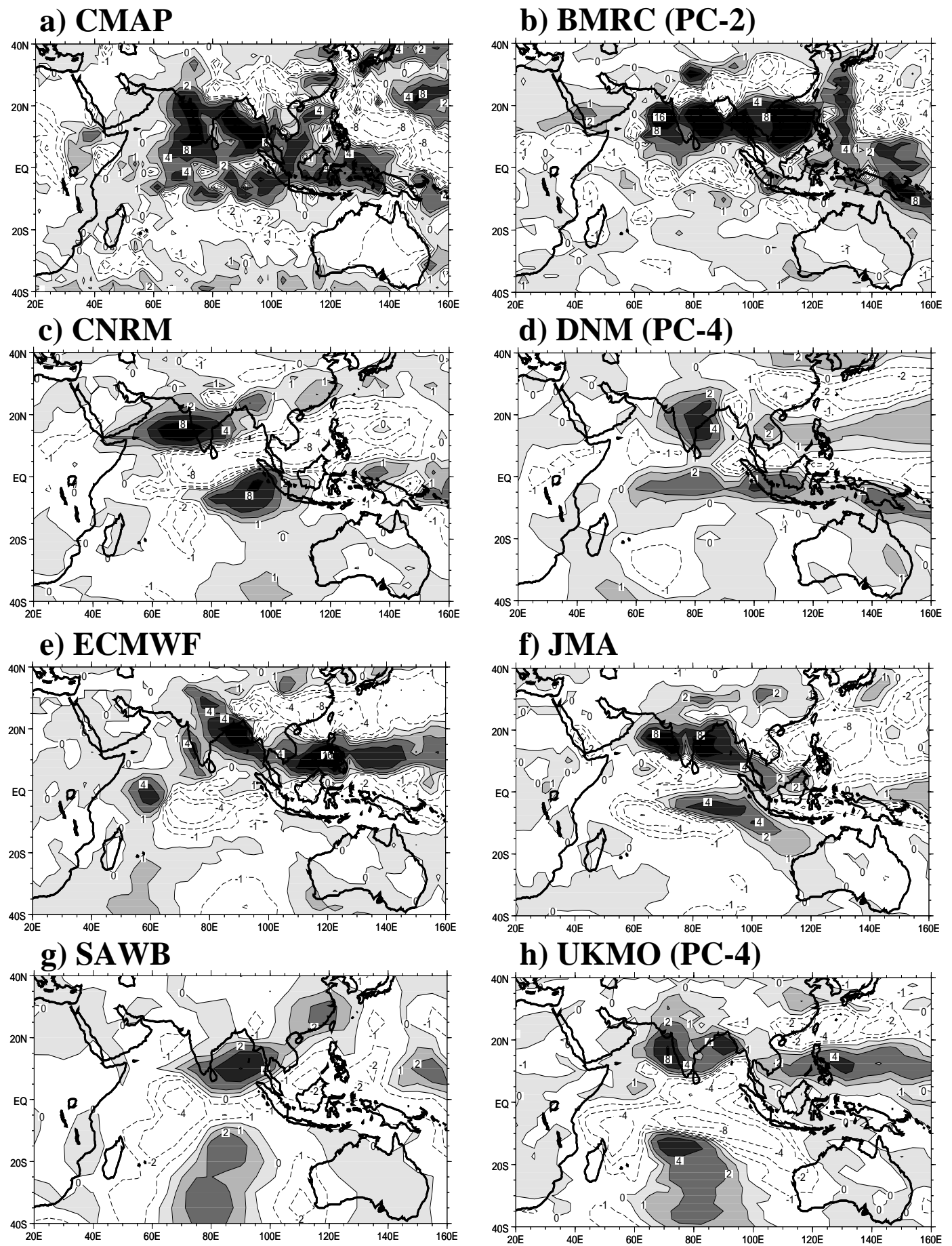
Figure 8: As Fig. 6 for EOF-3/PC-3.

vicinity of India. DNM (Fig. 8d) performs well over the Indian subcontinent, but the negative rainfall anomalies to the south are displaced substantially westward, consistent with errors in the location of the anticyclone (Fig. 5d). SAWB (Fig. 8g) exhibits an eastward displacement of positive rainfall anomalies into the Bay of Bengal. Consistent with its reasonable simulation of the low-level flow east of 100°E, JMA (Fig. 8f) best represents the southeastward tilt of the rainfall into the western Pacific, but the anomalies are too weak, and the model incorrectly simulates below-normal rainfall over the South China Sea. BMRC (Fig. 8b) exhibits a southeastward tilt to the enhanced rainfall anomalies, but the flow in this region is incorrectly simulated (Fig. 5b).

The models are most adept at simulating EOF-1 and its associated rainfall anomalies. For the higher order modes regional differences relative to the observations become more manifest, with the most substantial errors occurring east of 100°E. Overall the most realistic models are CNRM, ECMWF, JMA, and UKMO. BMRC exhibited substantial shifts over the Indian longitudes, and DNM and SAWB, the coarse resolution models, exhibited difficulty in capturing the sharp gradients seen in the reanalysis. Thus, while it may be possible for some of the models to simulate large-scale patterns of rainfall anomalies, the regional differences relative to the observations suggest that accurate hindcasts of the magnitude and regionality of rainfall anomalies will be problematic. This is especially noticeable in the case of the rainfall associated with EOF-1/PC-1 from the BMRC, DNM (EOF-7/PC-7), ECMWF, and SAWB models (Figs. 6b, d, e, and g). The failure to capture the correct subseasonal rainfall signal over India has direct implications for forecasts/hindcasts of interannual variability. Even with a correct projection of EOF/PC-1 onto the seasonal mean rainfall, the rainfall over India due to this mode will be incorrect. The projections of the subseasonal modes onto the interannual variability is discussed further in Section 5.

5. Subseasonal and interannual variability

a) Systematic perturbations of the modes
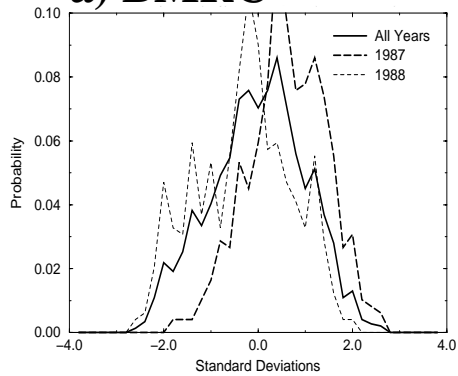
Early work with a simple model to illustrate the paradigm of external forcing systematically perturbing chaotic variability (Palmer 1994), and a simple coupled model of summer monsoon (Webster et al. 1998) suggested that forced perturbations would be manifest as bimodality of the probability distribution function (PDF) of the principal component timeseries. Bimodality is an indication that the residence time of a mode in either state is longer than the time for the transition between the states. However, using the reanalysis data, Sperber et al. (2000) found that the perturba-
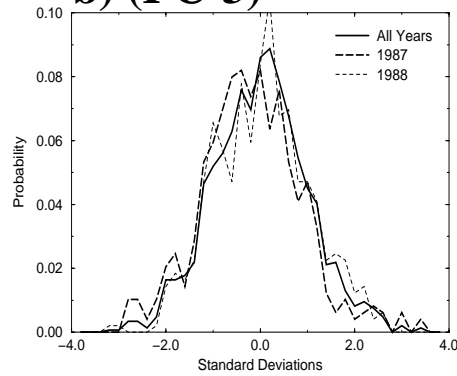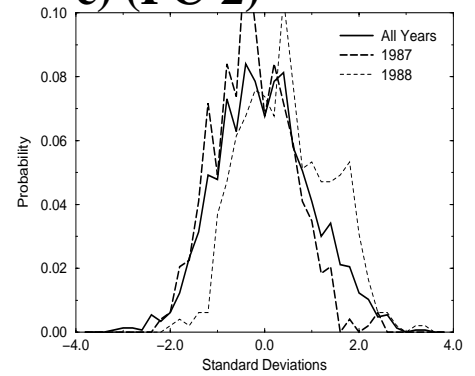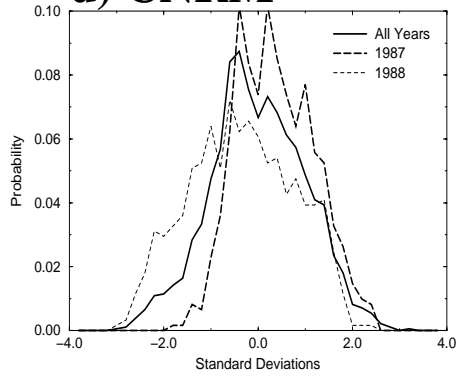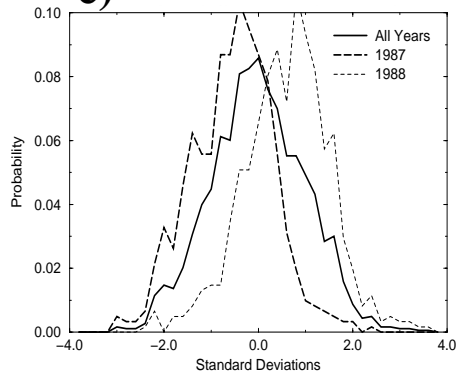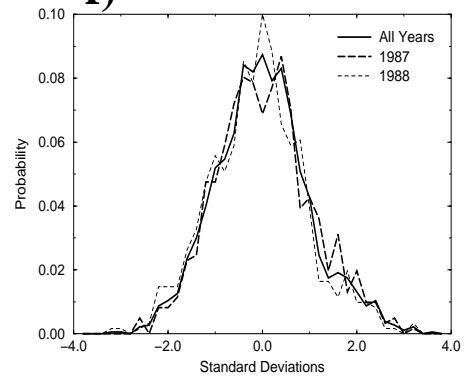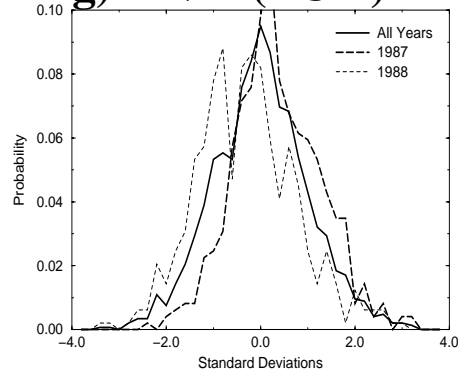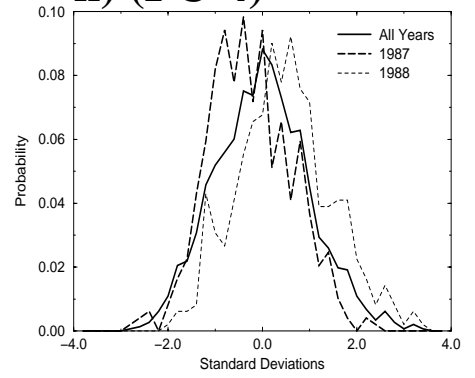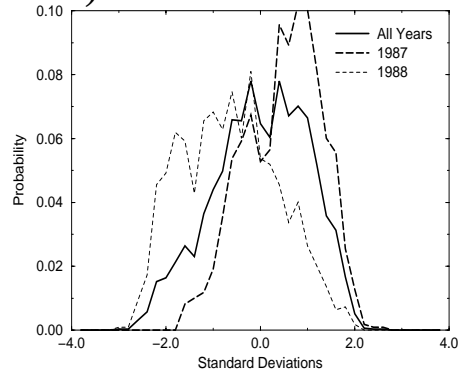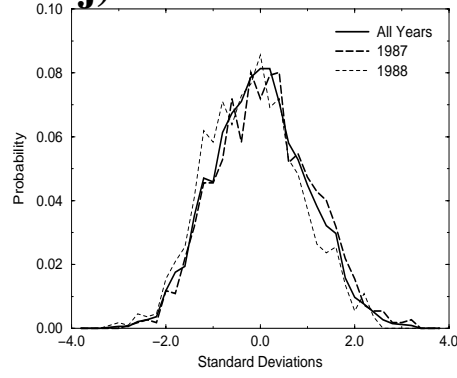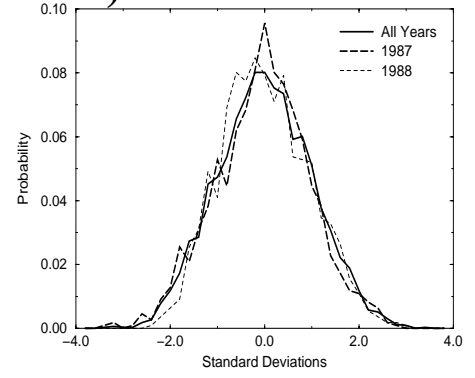
Figure 9: Probability distribution functions (PDF's) of the principal component time series of EOF's 1-3 given in Figs. 3-5. Each of the principal component time series were standardized prior to calculating the PDF's. The solid line is the PDF based on all years of data. The thick dashed line is the PDF for 1987, and the thin short-dashed line is the PDF for 1988.

PC-1

l) JMA

o) SAWB

r) UKMO

PC-2

m)

p)

s)

PC-3

n)

q)

t) (PC-4)
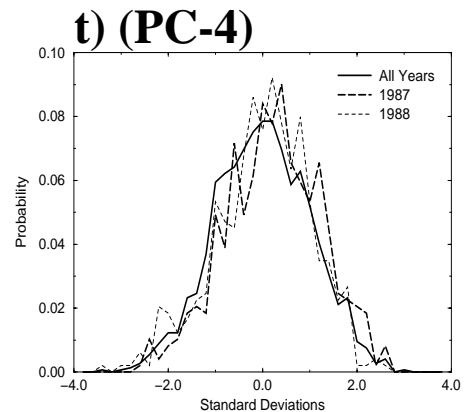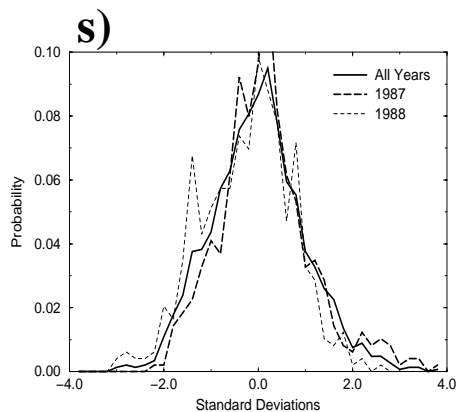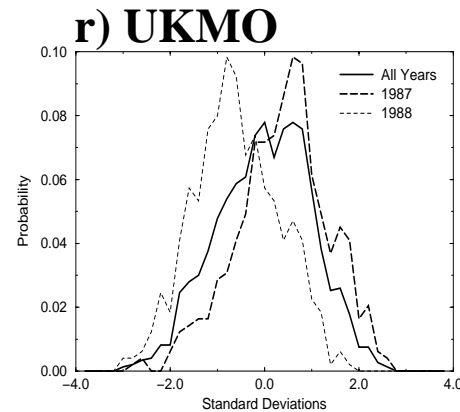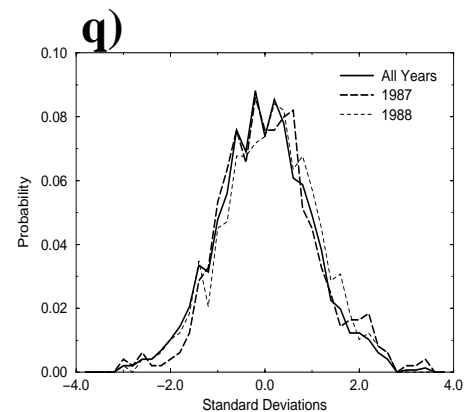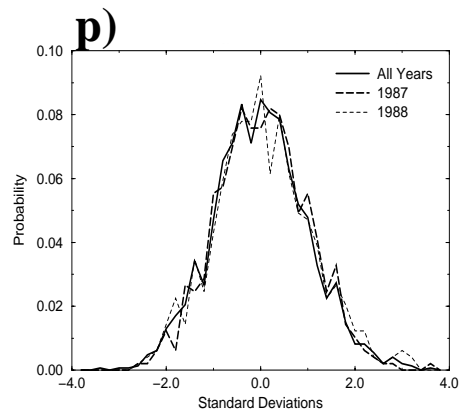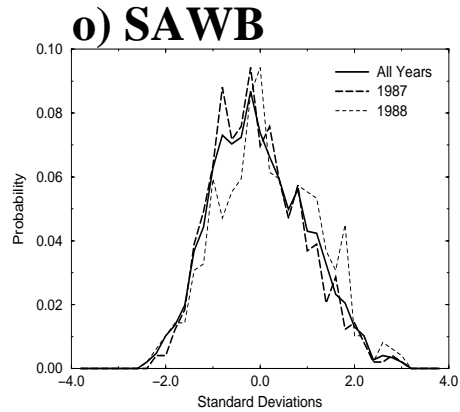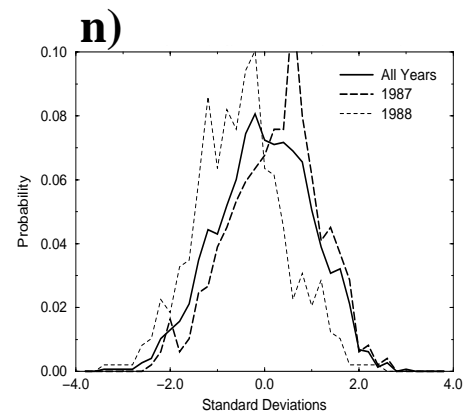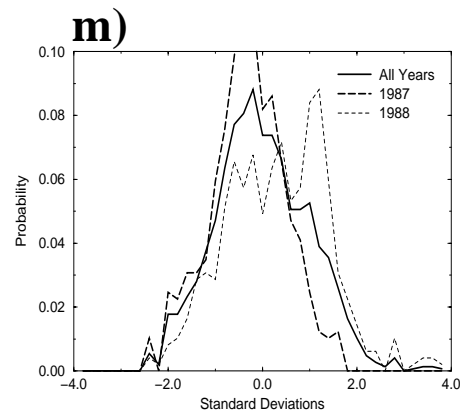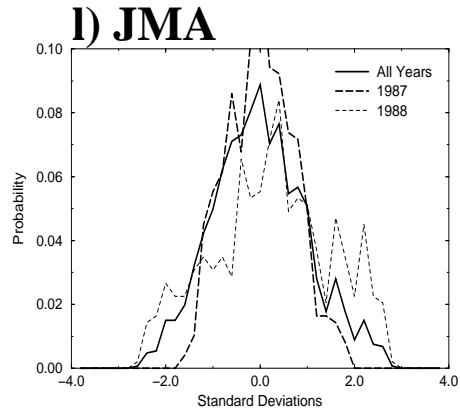
Figure 9 (con't)

tions of ASM subseasonal variability were manifested as changes in the means of gaussian PDF's, indicating that the residence time is of the same order as the transition time. If the models do not simulate gaussian PDF's this would indicate that they are not capturing crucial characteristics of the temporal variability of the modes. Furthermore, predictability of the ASM has its inherent limitations since only a few of the observed modes exhibit systematic perturbations.

As shown by Sperber et al. (2000), EOF-1/PC-1 is chaotic with respect to the phase of ENSO, strong vs. weak year of all-India rainfall (AIR), strong vs. weak years of the dynamical windshear index (DMI; Webster and Yang 1992), and the interdecadal variability of the land-sea temperature contrast over the monsoon region. This of course limits predictability of the ASM, since random perturbations of the dominant mode will compromise DSP. EOF-2 was systematically perturbed according to the phase of ENSO, with the mean of the probability distribution function (PDF) of PC-2 being negative during El Niño and positive during La Niña. However, it was noted that 1988 was an exception to this finding with the projection of EOF-2/PC-2 being negative during 1988, attesting to the predictability being necessarily probabilistic rather than deterministic. EOF-3/PC-3 is systematically perturbed with respect to AIR, the mean of the PDF of PC-3 being positive (negative) during years of above- (below-) normal AIR. That EOF-3/PC-3 is not systematically perturbed by ENSO is consistent with the lack of a unique relationship between NINO3 SST and AIR over the period 1958-97, their correlation being -0.46 (Sperber et al. 2000). If the models do not simulate PDF's that exhibit the observed systematic perturbations, this indicates that the models are not producing observed teleconnections to the boundary forcing, possibly related to shortcoming in model physics, thus further compromising DSP.

The PDF's of the modes given in Figs. 3-5, are shown in Fig. 9. The thick solid line is the PDF based on all ensemble members for 1987, 1988, and 1993. The shape of the PDF's are essentially gaussian, in agreement with the shapes of the observed PDF's in Sperber et al. (2000). Additionally, stratification is performed with respect to 1987 (thick long-dashed line) and 1988 (thin short dashed line), corresponding to years of below-normal and above-normal AIR. Based upon the results of Sperber et al. (2000), as discussed above, agreement with observations would result if the models exhibited a change in the mean of the PDF of PC-3 such that the mean is negative during 1987, and positive during 1988. Changes in the means of the PDF's are assessed as in Sperber et al. (2000) by use of a two-tailed t-test which takes into account serial correlation for the estimation of the number of degrees of freedom. For PC-3 (from the reanalysis), BMRC (PC-2), DNM (PC-4) and JMA (Figs. 9c, h, and n) exhibit

systematic changes in the means of the PDF's based on the t-test at the 5% significance level. BMRC and DNM correctly simulate the observed perturbation, while JMA incorrectly yields the mean of the PDF to be positive (negative) during 1987 (1988). Although this model gave an excellent representation of EOF-3 (Fig. 5f) and was able to establish the subseasonal link of this mode to rainfall (Fig. 8f), especially over India, it does not properly project this mode onto interannual variability of the ASM.

The most demonstrative error among the models is their propensity for producing systematic perturbations to PC-1, contrary to the results of Sperber et al. (2000) who found no perturbations of this mode with respect to AIR, ENSO, DMI, etc.. The simulated perturbations of this mode will contribute to poor hindcasts of the interannual rainfall variability. BMRC, CNRM, DNM (PC-7), ECMWF, and UKMO (Figs. 9a, d, g, i, and r) all indicate the mean of the PDF in 1987 to be greater than the mean of the PDF for 1988 for the t-test at the 5% significance level. Thus, these models exhibit unrealistically robust perturbations to the TCZ due to the link of this mode to the subseasonal variation of rainfall (Fig. 6). Additionally, CNRM and JMA (Figs. 9e and m) indicate PC-2 to be positive in 1988 contrary to the analysis by Sperber et al. (2000, their Table 2). The El Niño forcing in 1987 is consistent with the systematic negative perturbation to PC-2 in Sperber et al. (2000).

The results of the PDF's are encouraging in that they are basically gaussian, consistent with reanalysis (Sperber et al. (2000). Unfortunately, the simulated PDF's do not have the correct sensitivity to the boundary forcing on interannual timescales indicating that predictability will typically be poor. The PDF's are however based upon all members of the ensembles, and it possible that individual members may exhibit better agreement with observations.

As discussed in Sperber et al. (2000), the seasonal averages of the PC time series give the projections of the subseasonal modes onto the interannual variability. The projections of the reanalysis and the ensemble members from each model are given in Tables 2-8. A result of Sperber et al. (2000) is that 1987 should be the most predictable via EOF-2 and EOF-3 due to the presence of El Niño forcing and below-normal AIR. 1988 and 1993 should exhibit predictability through EOF-3. In the next subsections we evaluate the models abilities to hindcast the summer monsoons of 1987, 1988, and 1993. However, given the poor agreement of the simulated PDF's and their systematic perturbations with observations, DSP will be severely limited.

Table 2: Seasonal means (June-September) of the principal components (PC's) of the daily 850hPa wind for 1987, 1988 and 1993 from reanalysis and the BMRC ensembles. The dates indicate the start dates of the integrations. The seasonal means of the PC's give the projection of each mode onto the interannual variability. Shading indicates ensemble members that captured the correct sign of the observed projections for that year (see text for details).

Year	Source	$\overline{PC\text{-}1}$	$\overline{PC\text{-}2}$*	$\overline{PC\text{-}3}$#
1987	**NCEP**	**-2.5**	**-1.8**	**-14.3**
	ERA	**-1.6**	**-2.4**	**-6.5**
29 May	BMRC	13.7	-8.8	-11.7
30 May	BMRC	32.8	-5.6	-7.0
31 May	BMRC	12.3	-5.0	-6.4
1 June	BMRC	32.2	-0.4	-5.0
1988	**NCEP**	**-7.6**	**-1.3**	**10.8**
	ERA	**-5.9**	**-1.4**	**5.3**
29 May	BMRC	-28.5	4.1	10.1
30 May	BMRC	-5.6	3.7	15.9
31 May	BMRC	-25.9	-6.0	15.6
1 June	BMRC	15.3	2.2	15.3
1993	**NCEP**	**10.1**	**3.1**	**3.5**
	ERA	**7.5**	**3.7**	**1.2**
29 May	BMRC	6.9	6.1	-10.4
30 May	BMRC	-35.2	2.6	-13.7
31 May	BMRC	-9.1	7.8	-10.6
1 June	BMRC	-8.8	-0.9	8.0

*$\overline{PC\text{-}3}$ from BMRC
#$\overline{PC\text{-}2}$ from BMRC

Table 3: As Table 2 for CNRM.

Year	Source	PC-1	PC-2	PC-3
1987	**NCEP**	**-2.5**	**-1.8**	**-14.3**
	ERA	**-1.6**	**-2.4**	**-6.5**
28 May	CNRM	9.0	-20.9	-2.9
29 May	CNRM	11.4	-18.1	3.9
30 May	CNRM	7.6	-10.0	4.1
31 May	CNRM	32.1	-14.5	1.9
1 June	CNRM	7.0	-21.6	-1.0
1988	**NCEP**	**-7.6**	**-1.3**	**10.8**
	ERA	**-5.9**	**-1.4**	**5.3**
28 May	CNRM	-25.5	11.5	-6.6
29 May	CNRM	-14.3	30.8	-2.8
30 May	CNRM	-25.6	26.2	-3.7
31 May	CNRM	-21.6	23.6	-0.9
1 June	CNRM	24.4	2.3	1.0
1993	**NCEP**	**10.1**	**3.1**	**3.5**
	ERA	**7.5**	**3.7**	**1.2**
28 May	CNRM	-11.3	-3.6	2.3
29 May	CNRM	8.6	3.5	-3.5
30 May	CNRM	-10.5	0.8	1.6
31 May	CNRM	10.5	-2.6	5.2
1 June	CNRM	-1.8	-7.4	1.6

Table 4: As Table 2 for DNM. DNM did not simulate a counterpart to observed EOF-2.

Year	Source	PC-1*	PC-3^
1987	**NCEP**	**-2.5**	**-14.3**
	ERA	**-1.6**	**-6.5**
29 May	DNM	0.9	-3.0
30 May	DNM	4.2	0.1
31 May	DNM	0.0	-3.5
1 June	DNM	2.8	-1.2
1988	**NCEP**	**-7.6**	**10.8**
	ERA	**-5.9**	**5.3**
29 May	DNM	-1.2	3.8
30 May	DNM	-2.3	3.9
31 May	DNM	-0.9	2.6
1 June	DNM	-2.5	3.4
1993	**NCEP**	**10.1**	**3.5**
	ERA	**7.5**	**1.2**
29 May	DNM	0.0	-1.4
30 May	DNM	1.1	-0.9
31 May	DNM	-1.4	-3.5
1 June	DNM	-0.7	0.3

*$\overline{PC\text{-}7}$ from DNM
^$\overline{PC\text{-}4}$ from DNM

Table 5: As Table 2 for ECMWF.

Year	Source	PC-1	PC-2	PC-3
1987	**NCEP**	**-2.5**	**-1.8**	**-14.3**
	ERA	**-1.6**	**-2.4**	**-6.5**
23 May	ECMWF	26.3	7.5	-4.5
24 May	ECMWF	25.6	3.8	-1.2
25 May	ECMWF	17.5	-5.0	0.4
26 May	ECMWF	27.8	3.0	3.5
27 May	ECMWF	16.9	-3.2	-3.9
28 May	ECMWF	4.5	-0.9	1.1
29 May	ECMWF	40.2	5.2	-2.1
30 May	ECMWF	0.7	3.1	-0.4
31 May	ECMWF	24.9	5.1	-1.7
1988	**NCEP**	**-7.6**	**-1.3**	**10.8**
	ERA	**-5.9**	**-1.4**	**5.3**
23 May	ECMWF	-26.5	9.0	13.1
24 May	ECMWF	-15.0	3.4	3.2
25 May	ECMWF	-37.2	-10.1	-5.8
26 May	ECMWF	-46.2	-1.5	-2.8
27 May	ECMWF	-56.0	-3.8	-2.2
28 May	ECMWF	-2.6	-5.2	5.5
29 May	ECMWF	6.3	-22.5	-12.6
30 May	ECMWF	-27.6	-1.1	2.8
31 May	ECMWF	-43.5	-1.3	0.9
1993	**NCEP**	**10.1**	**3.1**	**3.5**
	ERA	**7.5**	**3.7**	**1.2**
23 May	ECMWF	18.7	2.1	3.4
24 May	ECMWF	-9.3	-3.0	0.9
25 May	ECMWF	3.6	0.6	3.9
26 May	ECMWF	30.1	-8.7	-14.2
27 May	ECMWF	-10.5	6.0	6.9
28 May	ECMWF	-6.3	4.0	3.2
29 May	ECMWF	7.7	1.7	1.1
30 May	ECMWF	20.8	10.2	3.8
31 May	ECMWF	9.4	1.5	-2.4

Table 6: As Table 2 for JMA.

Year	Source	PC-1	PC-2	PC-3
1987	**NCEP**	**-2.5**	**-1.8**	**-14.3**
	ERA	**-1.6**	**-2.4**	**-6.5**
29 May	JMA	15.0	-8.1	15.8
30 May	JMA	14.7	-4.5	1.3
31 May	JMA	-3.7	-20.1	0.4
1 June	JMA	-23.6	-7.7	9.1
1988	**NCEP**	**-7.6**	**-1.3**	**10.8**
	ERA	**-5.9**	**-1.4**	**5.3**
29 May	JMA	49.9	15.6	-8.8
30 May	JMA	-40.6	2.1	-11.2
31 May	JMA	41.4	12.3	-24.2
1 June	JMA	-1.5	10.0	-18.9
1993	**NCEP**	**10.1**	**3.1**	**3.5**
	ERA	**7.5**	**3.7**	**1.2**
29 May	JMA	-28.5	2.3	15.4
30 May	JMA	-23.0	-8.8	2.0
31 May	JMA	-25.4	3.0	3.9
1 June	JMA	25.4	3.9	15.2

Table 7: As Table 2 for SAWB.
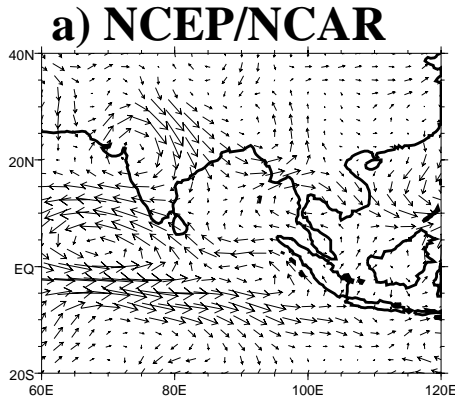
Year	Source	PC-1	PC-2	PC-3
1987	**NCEP**	**-2.5**	**-1.8**	**-14.3**
	ERA	**-1.6**	**-2.4**	**-6.5**
29 May	SAWB	-8.0	-1.2	2.5
30 May	SAWB	6.3	9.6	6.4
31 May	SAWB	0.7	5.1	3.7
1 June	SAWB	-3.1	3.9	8.3
1988	**NCEP**	**-7.6**	**-1.3**	**10.8**
	ERA	**-5.9**	**-1.4**	**5.3**
29 May	SAWB	-1.5	-2.6	1.0
30 May	SAWB	-3.1	-0.6	-2.7
31 May	SAWB	-1.2	-3.4	-2.7
1 June	SAWB	-2.3	-4.8	-2.2
1993	**NCEP**	**10.1**	**3.1**	**3.5**
	ERA	**7.5**	**3.7**	**1.2**
29 May	SAWB	2.3	-3.7	-2.8
30 May	SAWB	5.4	1.2	-1.6
31 May	SAWB	0.9	-2.0	-4.3
1 June	SAWB	3.7	-1.7	-5.7

Table 8: As Table 2 for UKMO.
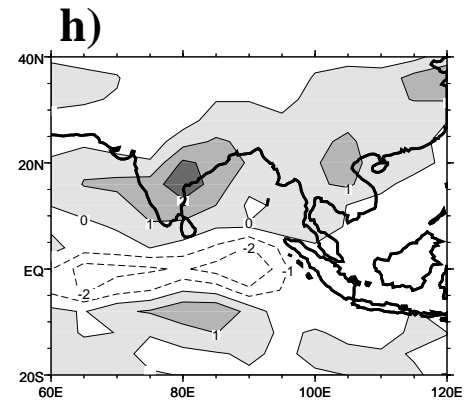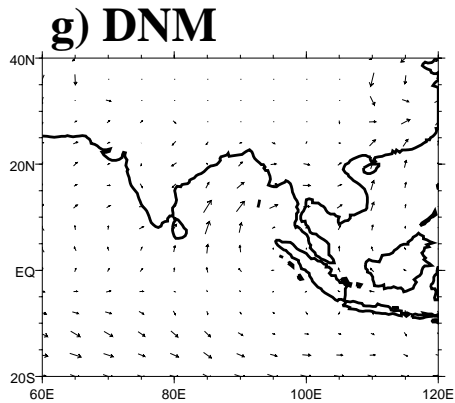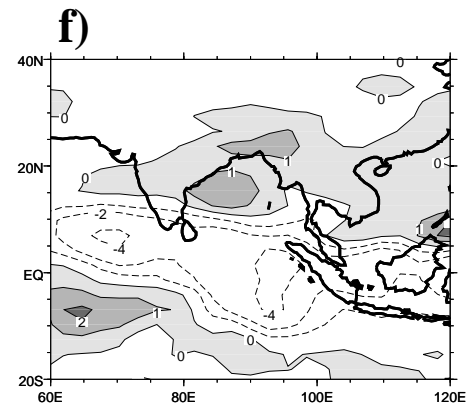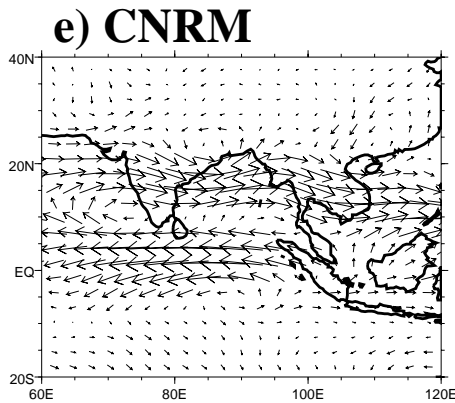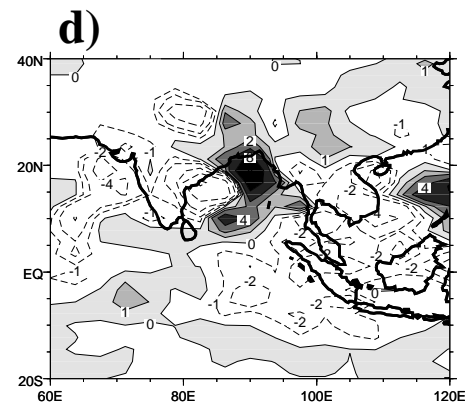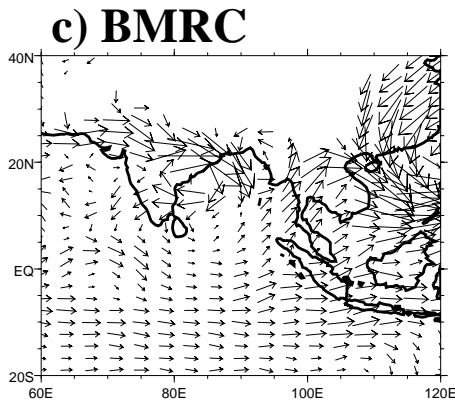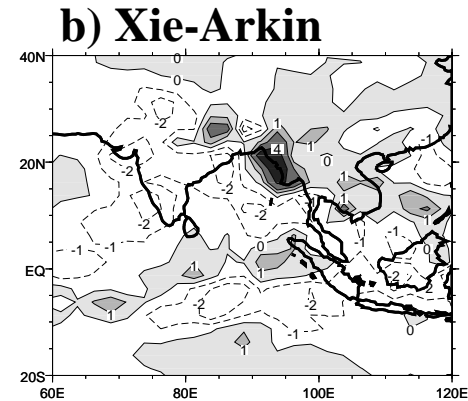
Year	Source	$\overline{PC\text{-}1}$	$\overline{PC\text{-}2}$	$\overline{PC\text{-}3}$*
1987	**NCEP**	**-2.5**	**-1.8**	**-14.3**
	ERA	**-1.6**	**-2.4**	**-6.5**
28 May	UKMO	19.2	6.0	1.8
29 May	UKMO	31.9	-5.7	14.0
30 May	UKMO	-8.8	12.0	2.0
31 May	UKMO	23.7	7.4	2.8
1988	**NCEP**	**-7.6**	**-1.3**	**10.8**
	ERA	**-5.9**	**-1.4**	**5.3**
28 May	UKMO	-26.1	-12.0	-2.5
29 May	UKMO	-32.8	0.5	0.6
30 May	UKMO	-27.2	-13.8	-5.7
31 May	UKMO	-18.2	-4.7	8.8
1993	**NCEP**	**10.1**	**3.1**	**3.5**
	ERA	**7.5**	**3.7**	**1.2**
28 May	UKMO	17.7	14.5	-5.9
29 May	UKMO	-11.8	-9.3	-2.0
30 May	UKMO	8.8	3.1	-6.7
31 May	UKMO	23.7	1.9	-7.4

*$\overline{PC\text{-}4}$ from UKMO

850hPa winds

a) NCEP/NCAR

c) BMRC

e) CNRM

g) DNM

Rainfall

b) Xie-Arkin

d)

f)

h)
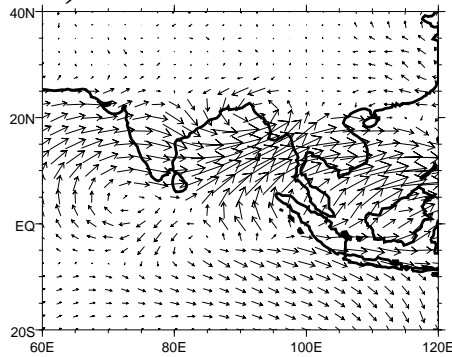
Figure 10: June-September averaged 850hPa wind and rainfall anomalies for 1987 relative to the base period 1987, 1988, and 1993. For the models, the anomalies are calculated using all ensemble members. Positive rainfall anomalies are shaded and the contour interval is +/-0, 1, 2, 4, 8,...mm day^{-1}. A unit vector corresponds to 2.5m s^{-1}.

850hPa winds

Rainfall

i) ECMWF

j)

k) JMA

l)

m) SAWB

n)
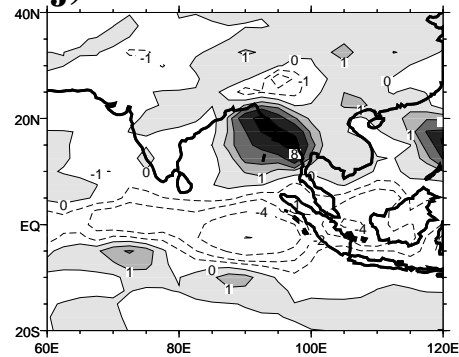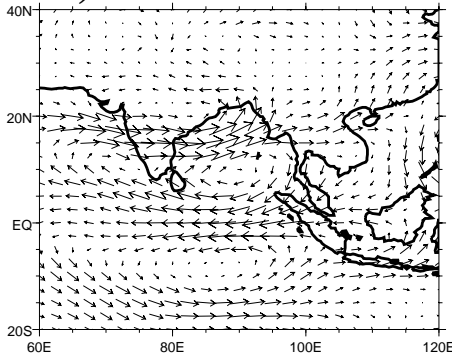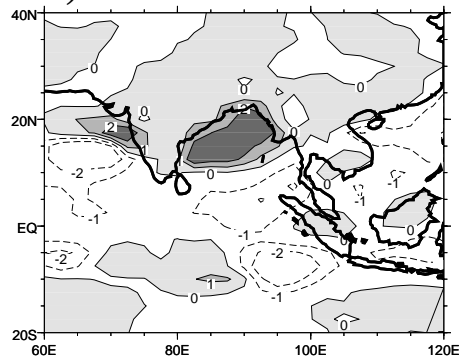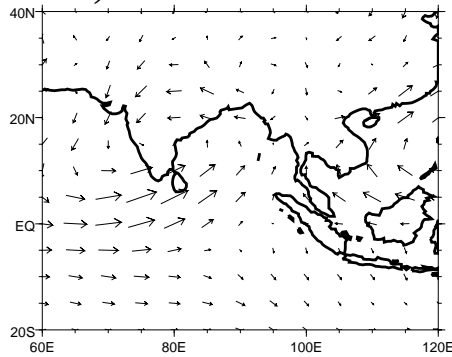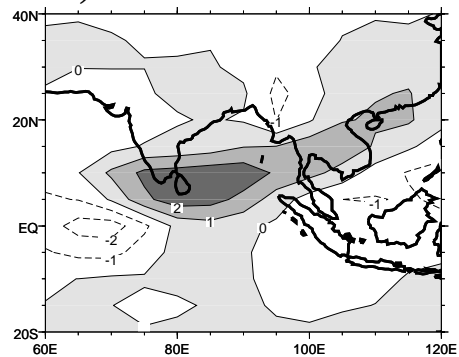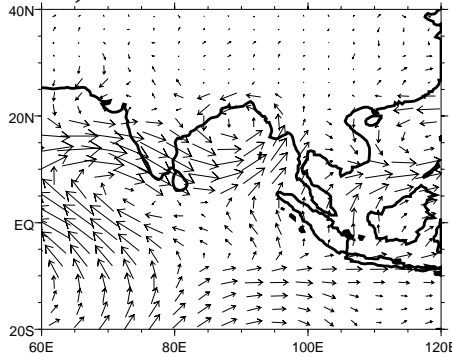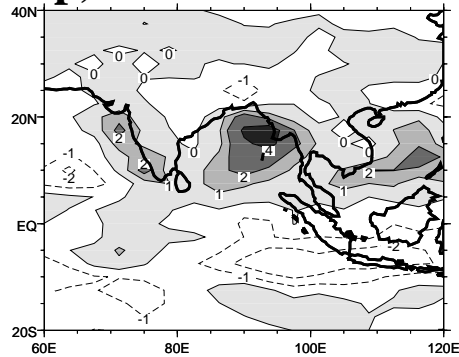
o) UKMO

p)

2.5

Figure 10 (con't)

b) 1987

Relative to the time-mean of 1987, 1988, and 1993, the seasonal mean (June-September) 850hPa wind anomalies and the Xie and Arkin (1996) rainfall anomalies for 1987 are shown in Figs. 10a and b. In the vicinity of India and the Bay of Bengal the anomalies are consistent with those presented in Sperber et al. (2000) relative to the 1958-97 wind climatology and the 1979-95 rainfall climatology. The anticyclonic anomalies over India are consistent with the negative projection of $\overline{PC\text{-}3}$ in the re-analysis (Table 2), and thus the negative rainfall anomalies over the Indian subcontinent. In conjunction with the negative loading of $\overline{PC\text{-}3}$, the negative projection of $\overline{PC\text{-}2}$ further enhances the northwesterly anomalies over northeast India. Negative projections of $\overline{PC's\ 1\text{-}2}$ are also associated with below-normal rainfall over India (the reverse of Figs. 6a and 7a). As discussed in Sperber et al. (2000), 1987 was an interesting year with the seasonal means of $\overline{PC's\ 1\text{-}3}$ all being negative, such that constructive interference of these modes gave rise to one of the strongest droughts of AIR. The enhanced rainfall near Burma (Fig. 10b) is associated with onshore flow from the northern Bay of Bengal, while in the near equatorial Indian Ocean (80^oE-100^oE) the enhanced rainfall is associated with the tendency for cyclonic anomalies (Fig. 10a).

To date, seasonal anomalies from simulations have been directly compared to those from observations. Regions of agreement and disagreement are usually discussed, but the phenomena contributing to the regionality is not typically explored. Our approach here is to interpret the anomalies with respect to the interactions of the dominant modes of subseasonal variability to ascertain if the anomalies thus simulated arise due to the correct interrelationships of the modes.

As seen in Fig. 10d, the BMRC model appears to have simulated a qualitatively realistic pattern of rainfall anomalies in 1987 over India and Burma, and similar to the reanalysis there are northwesterlies over northeast India and onshore flow near Burma. To the credit of the model, all ensemble members for 1987 simulate the correct sign of the projections of $\overline{PC\text{-}2}$ and $\overline{PC3}$ (Table 2), thus correctly contributing to the northwesterlies over northeast India and onshore flow near Burma, and the associated rainfall anomalies there. However, Table 2 indicates that $\overline{PC\text{-}1}$ is the dominant controlling mode for this models simulation of the 1987 ASM, with the projections being larger by a factor of 2-3 over $\overline{PC\text{-}2}$ and $\overline{PC\text{-}3}$. This is readily apparent with the 850hPa anomalies in Fig. 10c which very closely resemble those of EOF-1 (Fig. 3b), including the incorrectly simulated northwesterly anomalies over northeast India and the cyclonic anomalies over Burma. Thus, contrary to the observations in Table 2, the primary influence on ASM is through EOF-1 from the BMRC ensembles, indi-

cating that realistic rainfall anomalies from this model are strongly influenced by the incorrect representation of $\overline{\text{PC-1}}$.

For CNRM, Table 3 indicates that $\overline{\text{PC-2}}$ gives the dominant projection onto the seasonal anomaly, consistent with its negative PDF perturbation seen in Fig. 9e. This is reflected in the similarity of the total seasonal anomaly of the 850hPa flow (Fig. 10e) with the reverse of EOF-2 (Fig. 4c). These strong negative projections are consistent with the negative rainfall anomalies over southern India (Fig. 10f). The positive rainfall anomalies over central India arise due to the (incorrect) tendency for positive projections of $\overline{\text{PC-1}}$ and $\overline{\text{PC-3}}$, and their larger composite rainfall anomalies there (Figs. 6c and 8c).

The 850hPa wind anomalies for DNM in 1987 are very weak (Fig. 10g), with positive rainfall anomalies over the continental region (Fig. 10h). The correct negative projections of $\overline{\text{PC-4}}$ ($\overline{\text{PC-3}}$ from reanalysis) seen in Table 4, and the below-normal rainfall anomalies this mode indicates for India (the reverse of Fig. 8d) are counteracted by the incorrect positive projections of $\overline{\text{PC-7}}$ ($\overline{\text{PC-1}}$ in the reanalysis), and the other modes of subseasonal variability for which there are no counterparts in the reanalysis.

For the ECMWF model, the enhanced rainfall near Burma (Fig. 10j) is similar to observations, as is the limited area of below-normal rainfall over southern India. However, particularly over India, it is evident that the low-level wind anomalies (Fig. 10i) are not correctly simulated relative to observations (Fig. 10a). Rather, Table 5 indicates the presence of strong positive loadings of $\overline{\text{PC-1}}$ in 1987 in all but two members of the ensemble. These positive loadings are reflected in the close correspondence of the total seasonal anomaly of 850hPa wind (Fig. 10i) with EOF-1 (Fig. 3e) and the PDF perturbation seen in Fig. 9i. Thus, this mode contributes (incorrectly) to the negative rainfall anomalies over India due to the incorrect composite difference of rainfall seen over India in Fig. 6e. The positive loadings of $\overline{\text{PC-1}}$ are also associated with the enhanced rainfall at the head of the Bay of Bengal and the simulated cyclonic flow there, which in observations is predominantly due to the negative projection of $\overline{\text{PC-2}}$.

For JMA, Table 6 indicates that negative loadings of $\overline{\text{PC-2}}$ contribute to the enhanced rainfall over the northern Bay of Bengal (Fig. 10l), as does the overall positive loading (average over all ensemble members in 1987) of $\overline{\text{PC-1}}$ and the incorrect positive loading of $\overline{\text{PC-3}}$ (also noted in Fig. 9n). These latter two errors in the projection of subseasonal modes 1 and 3 also contribute to the incorrectly simulated enhanced rainfall over the continental regime of the ASM, and the incorrect low-level wind anomalies (Fig. 10k).

For SAWB, Table 7 indicates that $\overline{\text{PC-2}}$ and $\overline{\text{PC-3}}$ dominate, and that overall they have the incorrect loadings with respect to the observations. Consistent with this is the incorrect simulation of the seasonal anomalies of 850hPa flow and rainfall (Figs. 10m and n).

As with BMRC and ECMWF, the seasonal projection of $\overline{\text{PC-1}}$ from UKMO dominates (Table 8, and Fig. 9r), with the seasonal anomalies of 850hPa wind and rainfall (Figs. 10o and p) essentially corresponding to EOF-1 (Fig. 3h) and its associated composite difference of rainfall (Fig. 6h). Incorrectly simulated positive loadings of $\overline{\text{PC-2}}$ and $\overline{\text{PC-3}}$ also contribute to the failure of the model to capture the low-level wind and rainfall anomalies in 1987.

c) 1988
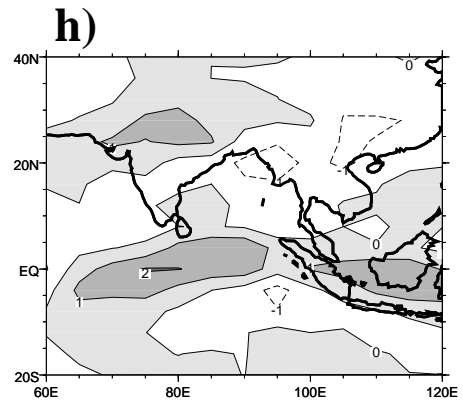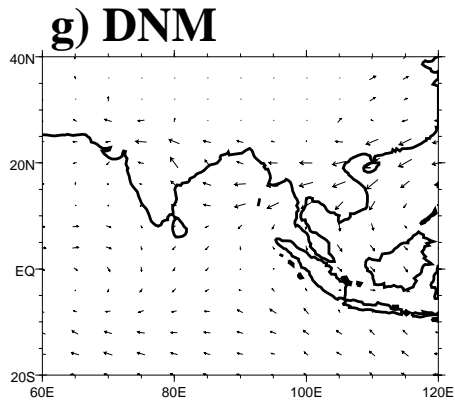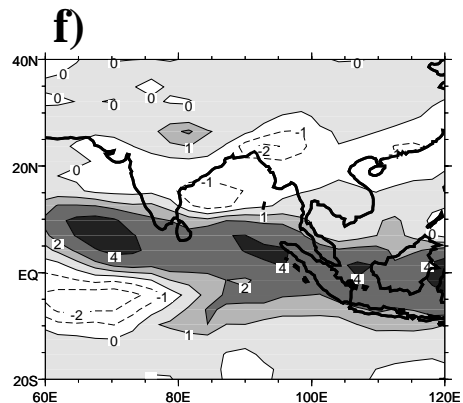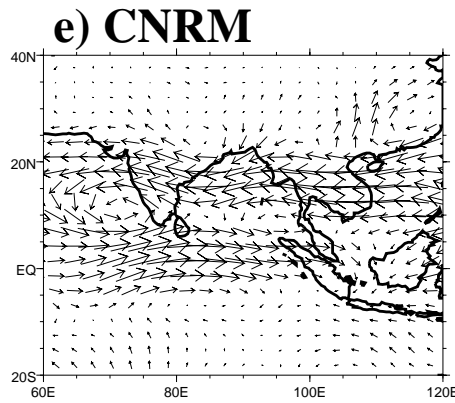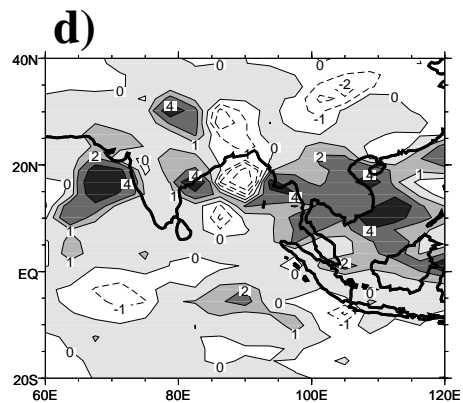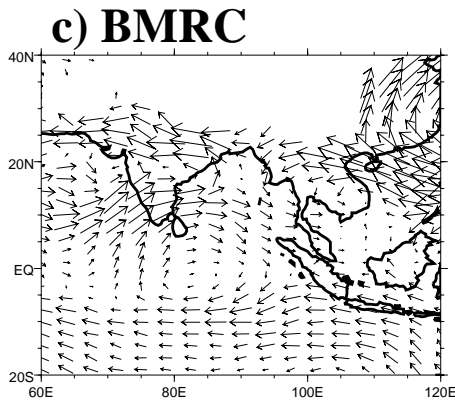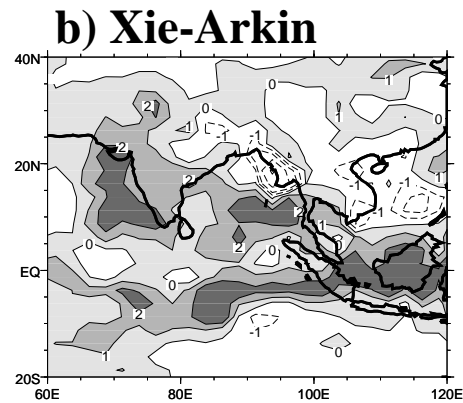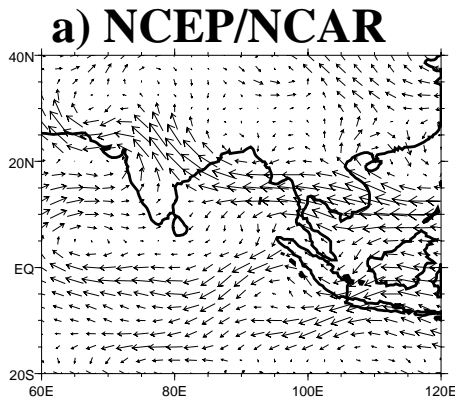
The 850hPa wind and rainfall anomalies for 1988, given in Figs. 11a-b, are mostly consistent with those relative to the longer record analyzed in Sperber et al. (1999). The exception is over the Arabian Sea where in the longer record the wind anomalies are easterly adjacent to the west coast of India, with below-normal rainfall west of the southern tip of India. This is due to the difference in the time-mean state (Figs. 1 and 2) relative to the longer climatologies used in Sperber et al (1999, 2000a). Even so, the comparison here is consistent since the same years are used for calculating the reference time-mean state for the models and observations. The spatial pattern of wind anomalies is nearly the opposite of that in 1987, consistent with the change in sign of the projection of $\overline{\text{PC-3}}$ onto the seasonal anomaly (Table 2). With disturbances along the monsoon trough, cyclonic anomalies near northwest India, and onshore flow near the western Ghats, enhanced rainfall dominates the Indian subcontinent and much of the Bay of Bengal.

BMRC is quite realistic in its' simulation of the 850hPa wind and rainfall anomalies, particularly near India and the Bay of Bengal (Figs. 11c and d). Importantly, this model simulates the positive projections of $\overline{\text{PC-3}}$ during 1987, consistent with observations. However, it must be noted that (on average) PC-1 is negative, and given the incorrect northward displacement of the westerlies over northern India (Fig. 3b), EOF-1 contributes excessively to the southwesterly anomalies over northeast India contrary to observations.

CNRM shows some elements of the low-level flow (Fig. 11e), in particular the tendency for southeasterly anomalies over northern India. Even so, the rainfall anomalies over the bulk of the Indian subcontinent are incorrectly simulated (Fig. 11f). As seen in Table 3, $\overline{\text{PC-2}}$ is strongly positive, contrary to observations, contributing to the

850hPa winds

a) NCEP/NCAR

Rainfall

b) Xie-Arkin

c) BMRC

d)

e) CNRM

f)

g) DNM

h)
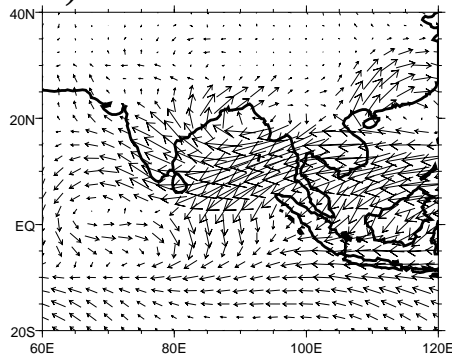
2.5

Figure 11: As Fig. 10 for 1988.

850hPa winds

Rainfall

i) ECMWF

j)

k) JMA

l)

m) SAWB

n)
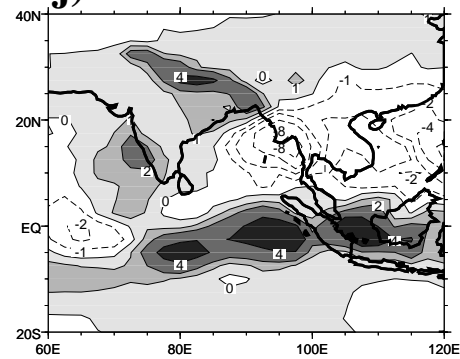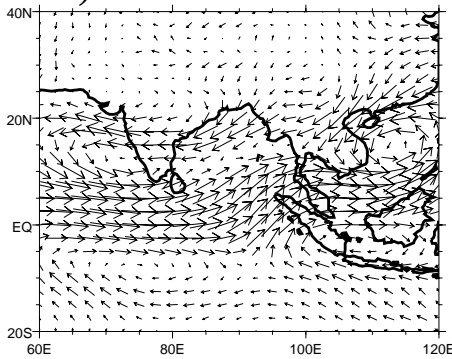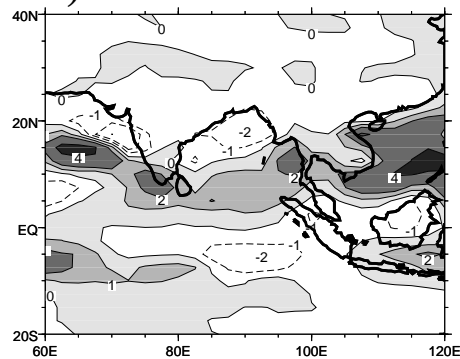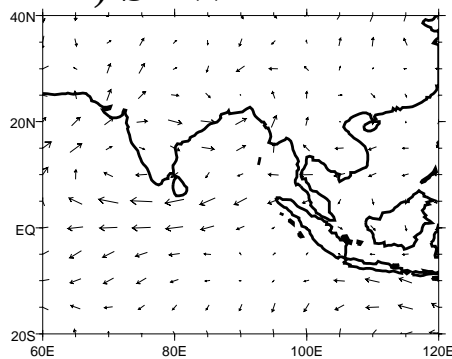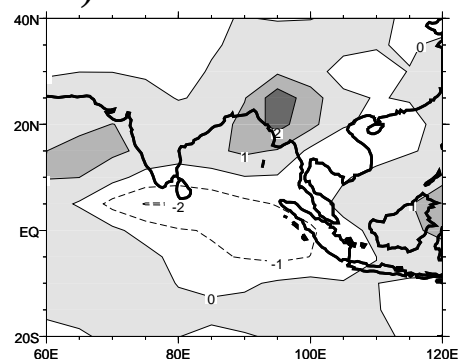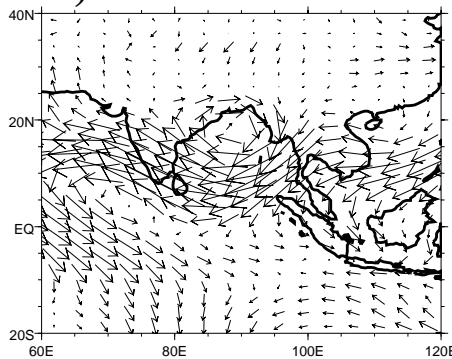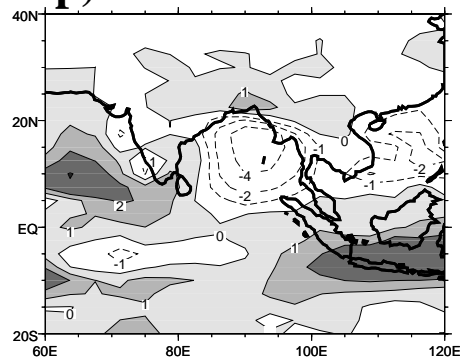
o) UKMO

p)

2.5

Figure 11 (con't)

enhanced rainfall near 10°N in the Indian Ocean. The predominantly negative loadings of $\overline{\text{PC-1}}$ are associated with the below-normal rainfall further north. Thus, this model fails to capture the important influence of $\overline{\text{PC-3}}$, and its associated enhancement of rainfall over India.

DNM has weak southeasterlies over northern India, and small positive rainfall anomalies there (Figs. 11g and h). This is consistent with the positive loadings of $\overline{\text{PC-4}}$ ($\overline{\text{PC-3}}$ from reanalysis) and the negative loadings of $\overline{\text{PC-7}}$ ($\overline{\text{PC-1}}$ from reanalysis. That the rainfall anomalies are not in better agreement with observations is due to the contribution from other subseasonal modes of variability (not shown).

The ECMWF model correctly simulates enhanced rainfall in the vicinity of India and the equatorial Indian Ocean (Fig. 11j). The southeasterly wind anomalies (Fig. 11i) over India are similar to observations, but the simulation lacks the onshore flow along the west coast of India seen in the reanalysis. Table 5 and Fig. 9i indicate that the flow anomalies are incorrectly dominated by negative loadings of $\overline{\text{PC-1}}$. Recalling that the rainfall anomalies associated with EOF-1/PC-1 (Fig. 6e) are incorrect over India, the negative loadings of $\overline{\text{PC-1}}$ incorrectly dominate the signature of enhanced rainfall over India. Thus, this model captures the correct rainfall signal due to an improper mix of projections, and the improper link between EOF-1/PC-1 and rainfall over India.

As seen in Table 6 for JMA, the projections of $\overline{\text{PC's 1-3}}$ on the seasonal anomalies are incorrectly simulated (averaged over all ensemble members), consistent with the poor simulation of the wind and rainfall anomalies in 1988 (Figs. 11k and l).

SAWB is similar to BMRC, DNM, and ECMWF in that negative loadings of $\overline{\text{PC-1}}$ (Table 7) contribute to enhanced rainfall over India (Fig. 11n) due to the incorrect rainfall pattern associated with this mode (Fig. 6g). Also, a strong contribution from a higher order mode (EOF-5/PC-5, not shown) contributes to the enhanced rainfall for the central and western portion of India. Thus, an improper mix of modes can give rise to a qualitatively correct rainfall signal, since as seen in Fig. 11m this model fails to capture the low-level convergence anomalies over the Indian subcontinent.

UKMO is similar to BMRC, DNM, ECMWF, and SAWB in that $\overline{\text{PC-1}}$ incorrectly dominates the projections onto the seasonal anomaly (Table 8). The overall negative loadings give rise to the southeasterly flow over India (Fig. 11o), and the tendency for negative rainfall anomalies over the Indian subcontinent (Fig. 11p).

850hPa winds

a) NCEP/NCAR

Rainfall

b) Xie-Arkin

c) BMRC

d)

e) CNRM

f)

g) DNM

h)

2.5
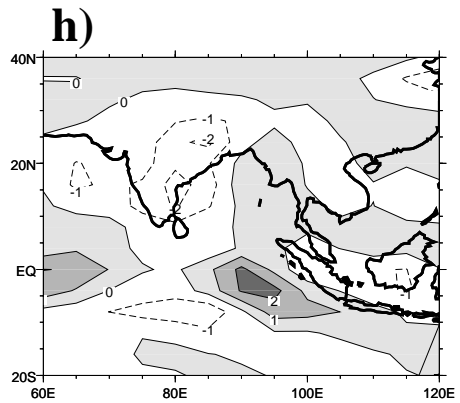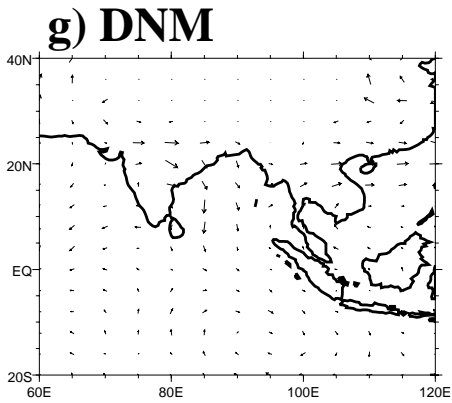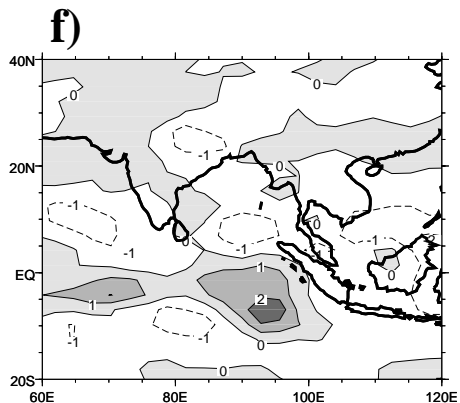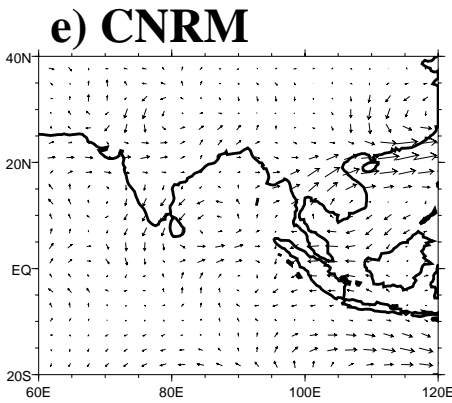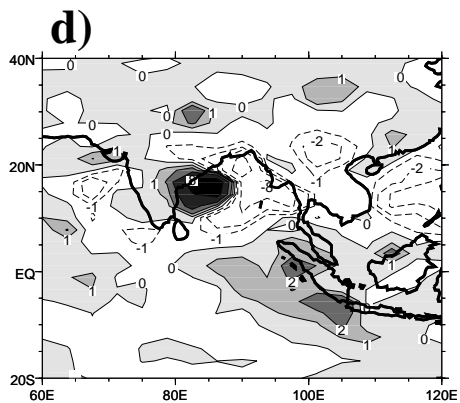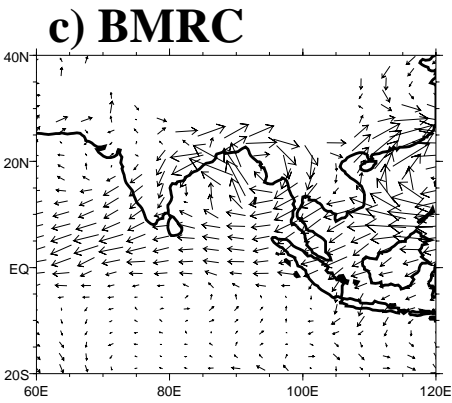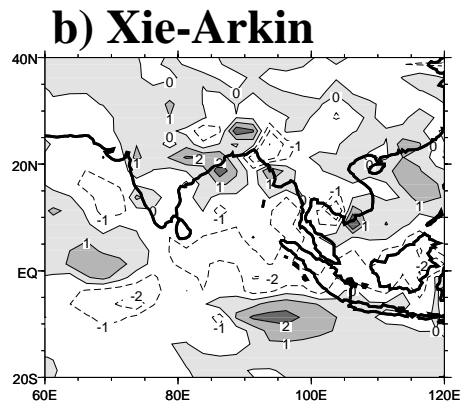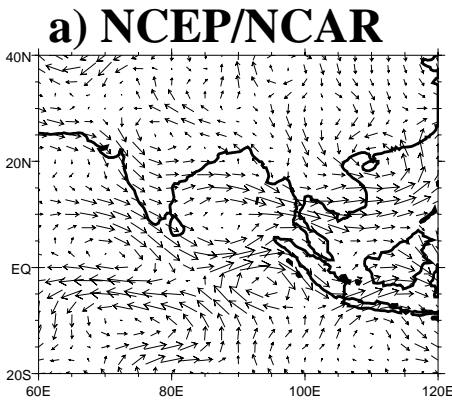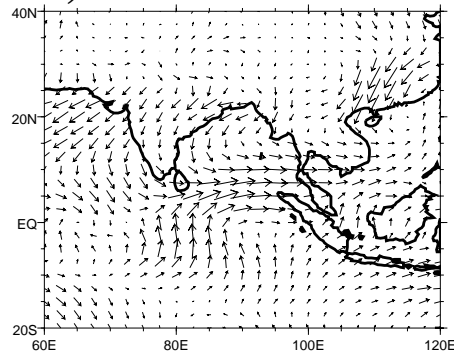
Figure 12: As Fig. 10 for 1993.

850hPa winds

Rainfall

i) ECMWF

j)

k) JMA

l)

m) SAWB

n)
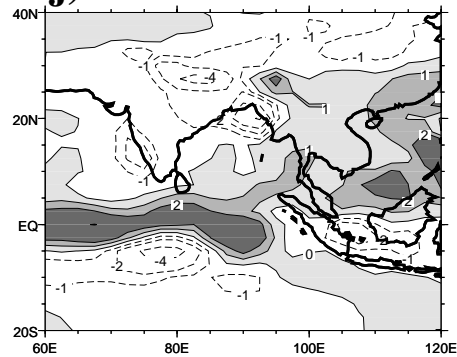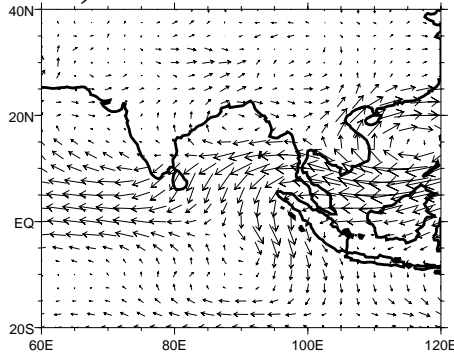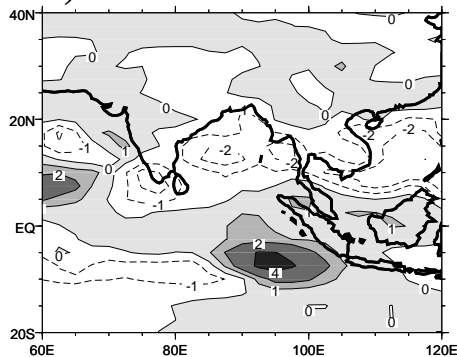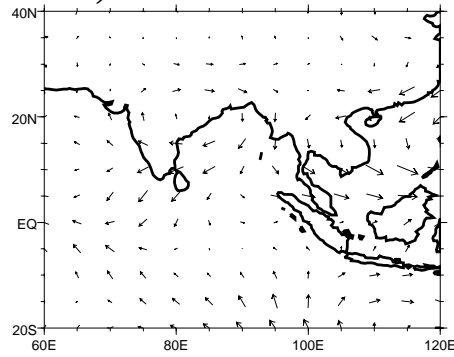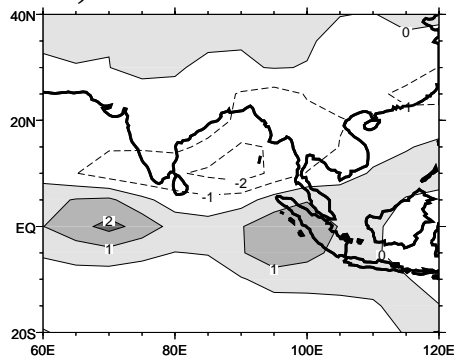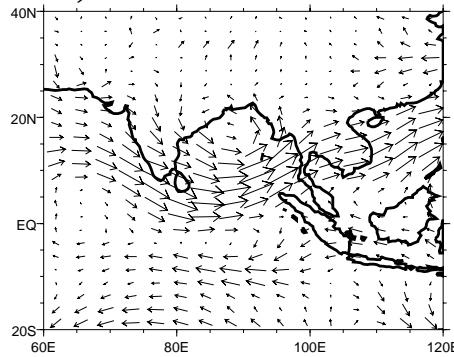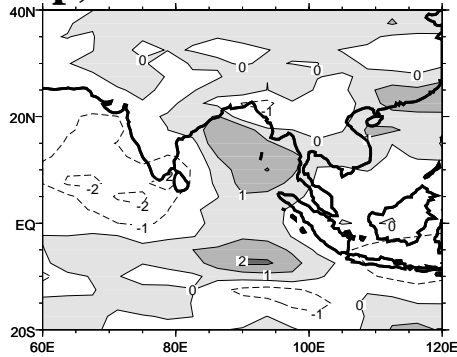
o) UKMO

p)

2.5

Figure 12 (con't)

d) 1993

The reanalyzed 850hPa wind anomalies in Fig. 12a primarily arise from the positive projection of $\overline{\text{PC-1}}$, as seen in Table 2. Consistent with this are the southeasterly anomalies over northeastern India, and the westerly anomalies along the west coast of India. The enhanced rainfall over western and northern India, and near the head of the Bay of Bengal, seen in Fig. 12b, are consistent with those relative to the longer base period 1979-95 (not shown).

For BMRC, the dominant negative loadings arise from $\overline{\text{PC-1}}$ and $\overline{\text{PC-2}}$ ($\overline{\text{PC-3}}$ from reanalysis) as seen in Table 2. Contrary to observations, the negative loadings of $\overline{\text{PC-1}}$ contribute to the enhanced rainfall over India due to the incorrect simulation of the rainfall response to this mode of variability (Fig. 6b). Thus, the enhanced rainfall over India arises from improper projections of the modes, and their error in simulating the proper subseasonal relationship with rainfall.

As seen in Table 3, the 1993 loadings for CNRM do not show any consistent preference for positive or negative loadings. As such the seasonal anomalies of 850hPa wind and rainfall are weak (Figs. 12c and d).

For DNM the westerly anomalies over northern India are associated with the incorrect negative loadings of $\overline{\text{PC-4}}$ ($\overline{\text{PC-3}}$ from reanalysis) as seen in Table 4. This contributes to the prevalence of negative rainfall anomalies over the subcontinent (the reverse of Fig. 8d). The poor precipitation response of EOF-7/PC-7 (EOF-1/PC-1 from reanalysis) also contributes to the poor signal in 1993, as does the models inability to generate the proper hierarchy of modes.

As seen in Table 5, ECMWF exhibits mixed signals in 1993, and for some of the realizations higher order modes dominate, unlike the observed projections. As such the 850hPa wind and the rainfall anomalies, given in Figs. 12i and j, are inconsistent with observations.

For JMA, the incorrect negative projections of $\overline{\text{PC-1}}$ for 3 of 4 members (Table 6) are further complicated by strong projections of higher order modes (not shown), thus resulting in the poor simulation of the 1993 anomalies (Figs. 12k and l).

Table 7 indicates that SAWB fails to capture the positive loadings of $\overline{\text{PC-2}}$ and $\overline{\text{PC-3}}$, and the relative importance of $\overline{\text{PC-1}}$ over $\overline{\text{PC-3}}$ seen in the reanalysis. As such the low-level wind and the rainfall anomalies are poorly represented (Figs. 12m and n).

As seen in Figs. 12o, the UKMO model gives a qualitatively correct representation of the wind anomalies in 1993. This is due to the correct signs of the projections of $\overline{\text{PC's 1-2}}$ in 3 of 4 members as seen in Table 8. The corresponding rainfall pattern

in Fig. 12p contains elements of the observed rainfall pattern, with the tendency for above-normal rainfall over northern India and below-normal rainfall to the south. The above-normal rainfall over northern India is not as coherent as observed since the model locates the cyclonic wind anomalies over the northwestern Bay of Bengal rather than over northern India.
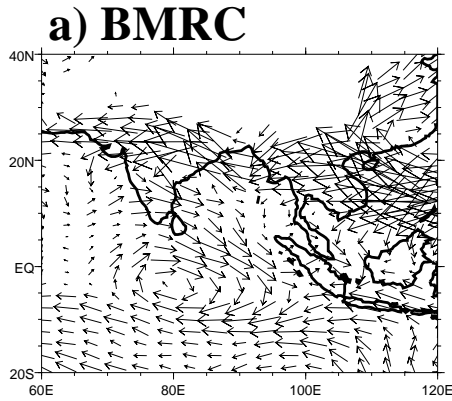
While the models have simulated the spatial patterns of the dominant subseasonal modes with varying degrees of fidelity, they are typically poor at representing the projections of the PC's onto the interannual variability. We have been able to highlight which modes contribute to errors in the simulation of the seasonal anomalies. Even though the first mode was determined to be chaotic with respect to ENSO, AIR, DMI etc. (Sperber et al. 2000), several models exhibit systematic perturbations of this mode (see Section 5a for more details), and they overestimate its influence relative to the other modes. All members of the BMRC and DNM ensembles have captured the proper projections of $\overline{\text{PC-3}}$ ($\overline{\text{PC-2}}$ and $\overline{\text{PC-4}}$ from BMRC and DNM) for 1987 and 1988, but errors in the simulation of the other modes dominate the seasonal anomalies such that in some cases a realistic pattern of rainfall anomalies is simulated but with a poor simulation of the 850hPa wind anomalies. In one case, JMA, all members had the incorrect sign of the projections of $\overline{\text{PC-3}}$ in 1987 and 1988, even though this model gave the best representation of EOF-3 (Fig. 5f). This highlights the importance of simulating the correct interannual projections of these modes. In the case of the boundary forced modes, such errors indicate that the model is failing to capture observed teleconnections.

Importantly, in 1987, as anticipated from the results of Sperber et al. (2000), $\overline{\text{PC-2}}$ should have negative loadings. Several of the models are adept at capturing this feature, including BMRC, CNRM, and JMA. In other cases, the incorrect representation of the $\overline{\text{PC-2}}$ loadings indicates that the models are not properly simulating ENSO/ASM teleconnections. It is possible that this is associated with poorly representing the location, magnitude, and/or vertical profile of the diabatic heating in the tropical Pacific associated with ENSO. Given the importance of simulating the interannual projections of the subseasonal modes the performance of the ensemble members will be analyzed by objectively by stratifying the integrations according to their projections onto the interannual variability.
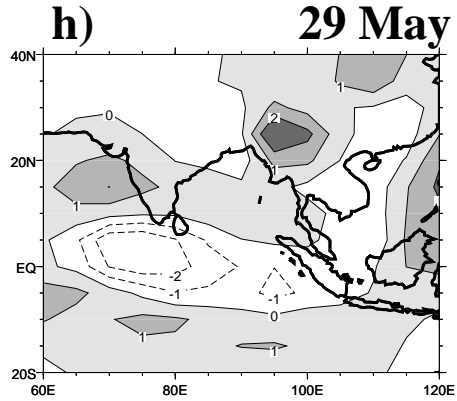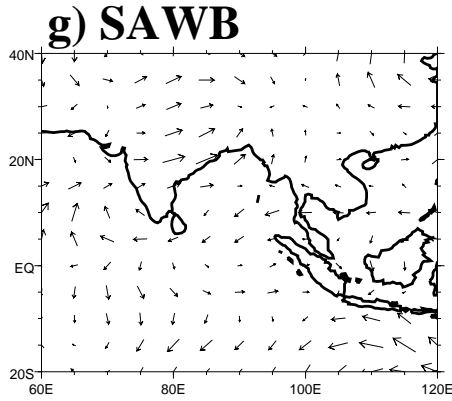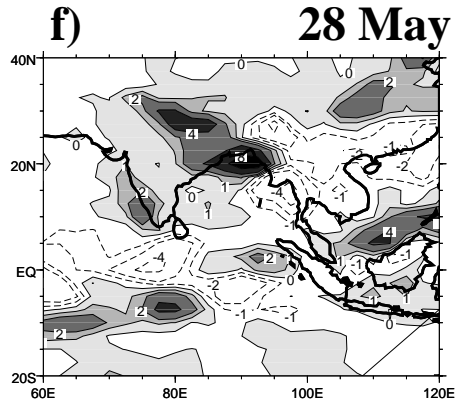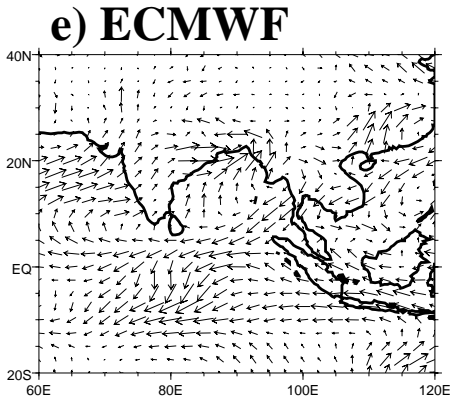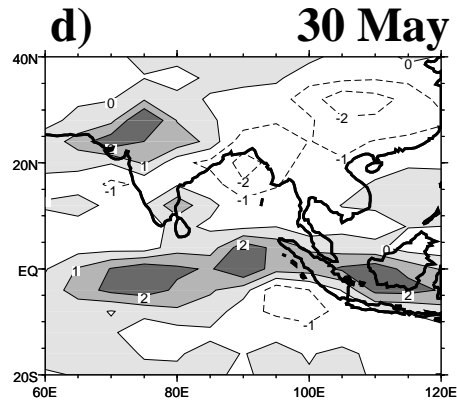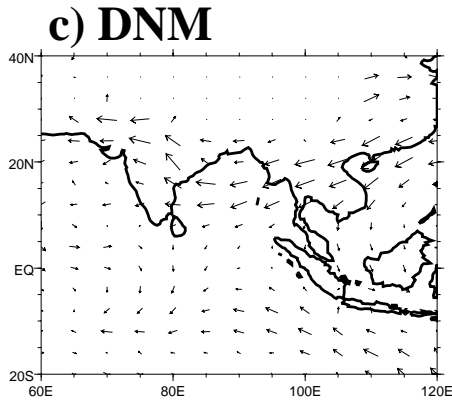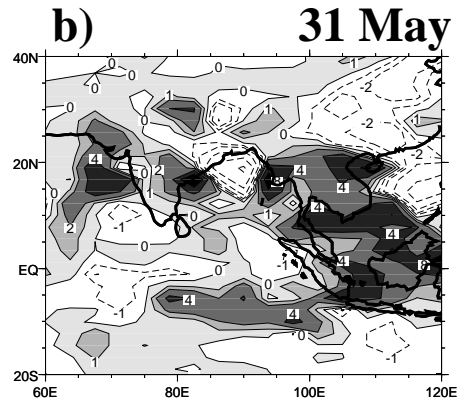
e) Objective performance of the ensemble members

We have shown that improperly simulating the projections of the subseasonal modes is associated with a poor representation of the interannual variability. To firm-

850hPa winds

Rainfall

a) BMRC

b) 31 May

c) DNM

d) 30 May

e) ECMWF

f) 28 May

g) SAWB

h) 29 May
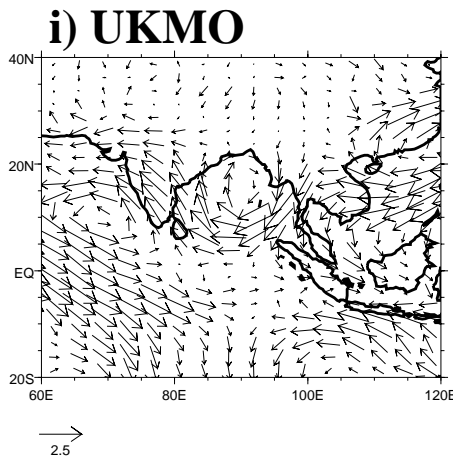
2.5

Figure 13: As Fig. 10, but for individual ensemble members for 1988. The indicated date(s) correspond(s) to the start date(s) of the integration(s). See text/tables for the selection criteria.

-43-

850hPa winds

### i) UKMO

Rainfall

j)   31 May
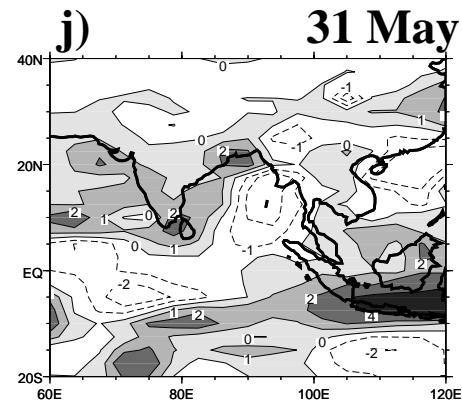
Figure 13 (con't)

ly conclude that the interactions of the subseasonal modes are important for the interannual variability we must demonstrate that proper projections result in an improved simulation of the interannual variability. This would also provide the added benefit of being able to objectively discriminate among the performance of the individual ensemble members.
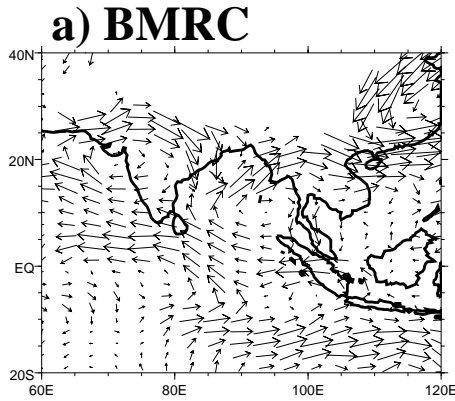
From examination of the Tables 2-8, none of the ensemble members were able to properly simulate the correct sign of the observed projections in 1987. However, in 1988 several of the models had at least one realization that was successful in this regard (see shaded entries in the tables). For BMRC, the 31 May 1988 integration simulates the correct signs of the observed projections of the subseasonal modes onto the interannual variability. The 850hPa wind and rainfall anomalies from this member (Figs. 13a and b) are amplified relative to the seasonal anomalies based on all members (Figs. 11c and d), mainly due to the strong negative projection of $\overline{PC\text{-}1}$, which as discussed earlier gives rise to excessively strong southeasterly anomalies due to the incorrect location of the westerly wind anomalies over India in EOF-1 (Fig. 3b), and the above-normal rainfall anomalies over India.

For DNM, the 30 May 1988 member has a reasonably realistic ratio between $\overline{PC\text{-}7}$ and $\overline{PC\text{-}4}$ ($\overline{PC\text{-}1}$ and $\overline{PC\text{-}3}$ from reanalysis), although the magnitudes of the projections are weak. The 850hPa wind and the rainfall anomalies associated with this member are given in Figs. 13c and d. Relative to the previously presented average over all members, Figs. 11g and h, the 30 May member exhibits more intense flow along the monsoon trough with a commensurate increase in the magnitude of the enhanced rainfall anomalies over India. Thus, the performance of this individual member exhibits a more realistic representation of the observed anomalies.

Figs. 13e-f show the anomalies from the 28 May 1988 ECMWF realization. Based on the data in Table 2, this member was chosen since it is not incorrectly dominated by $\overline{PC\text{-}1}$ whose rainfall signal over India was incorrect (Fig. 6b). In Fig. 13a there is an improved representation of the onshore flow adjacent to the west coast of India relative to Fig. 11i, but the southeasterlies in the vicinity of the monsoon trough are now absent. This is because the EOF-3 cyclone/anticyclone pattern (Fig. 5e) is shifted east of the observed location (Fig. 5a). Hence easterly anomalies are located just to the north of the Bay of Bengal rather than over northern India. This result indicates that it is important to minimize the systematic errors of the individual modes and to properly represent the partitioning of the loadings among the dominant modes.

From SAWB, the 29 May 1988 member has the most realistic projections of the $\overline{PC's}$ (Table 7), although the negative projection of $\overline{PC\text{-}1}$ still contributes to the en-

850hPa winds

Rainfall

a) BMRC

b)   29 May

c) CNRM

d)   29 May

e) DNM

f)   30 May

g) ECMWF

h)23, 25, 29-31 May

2.5
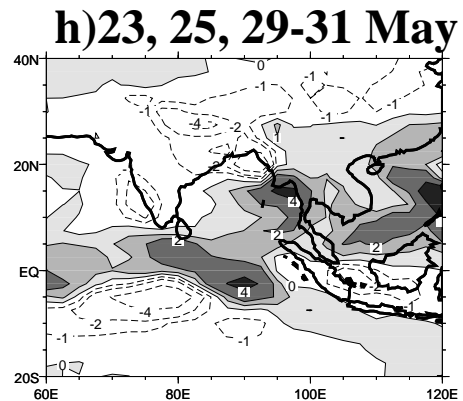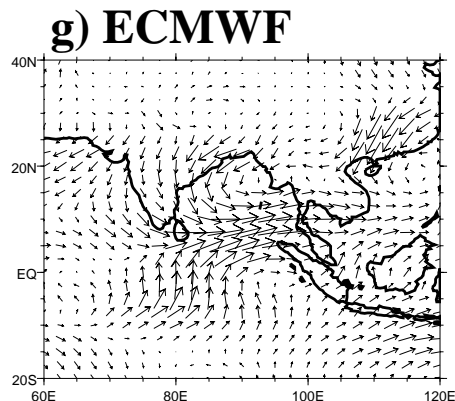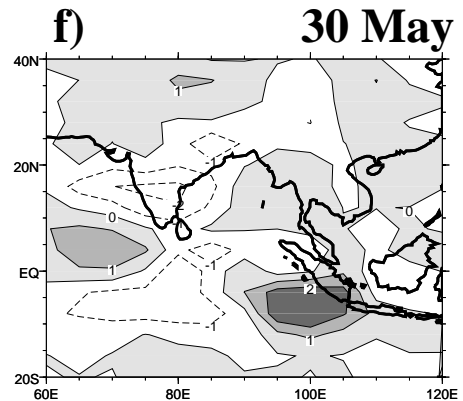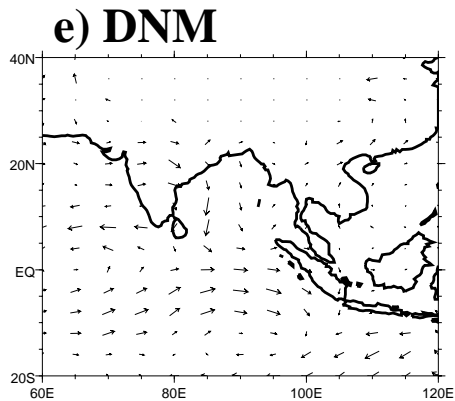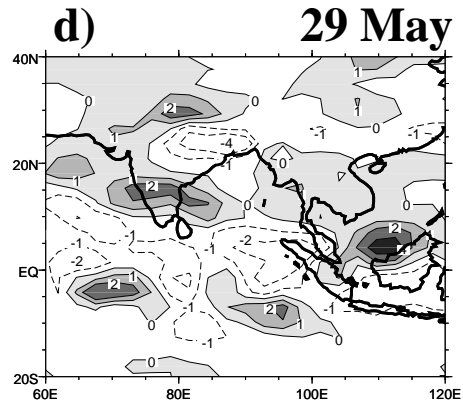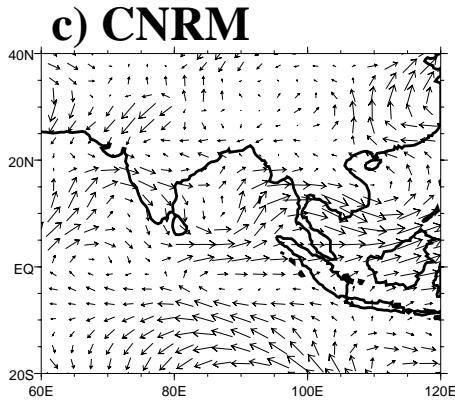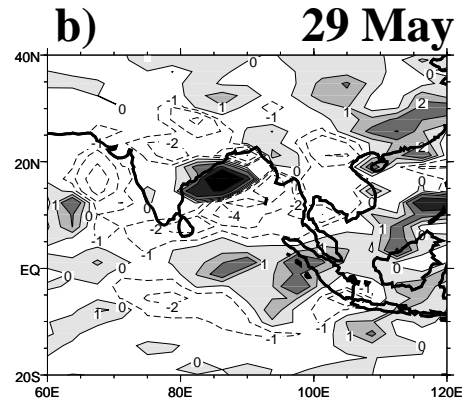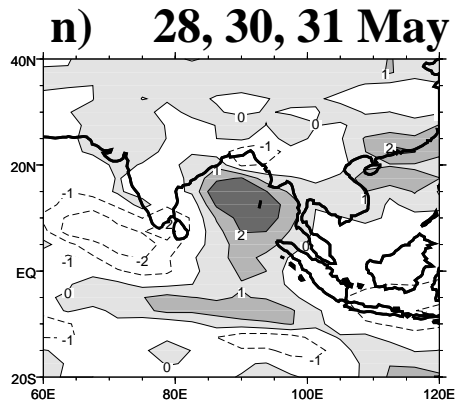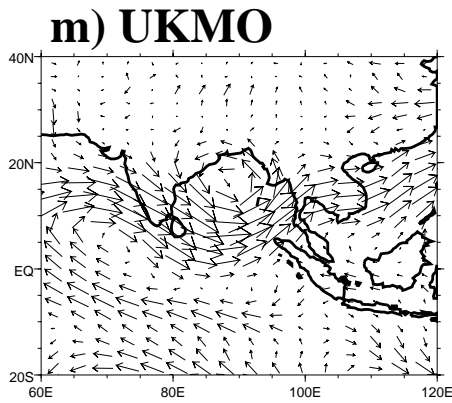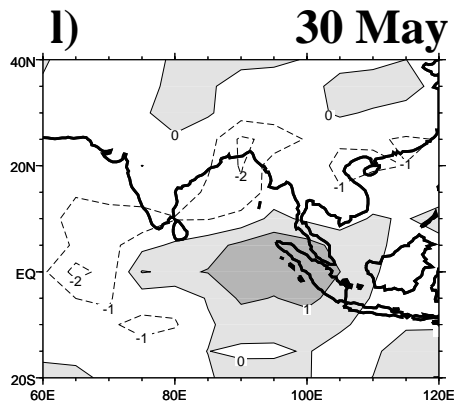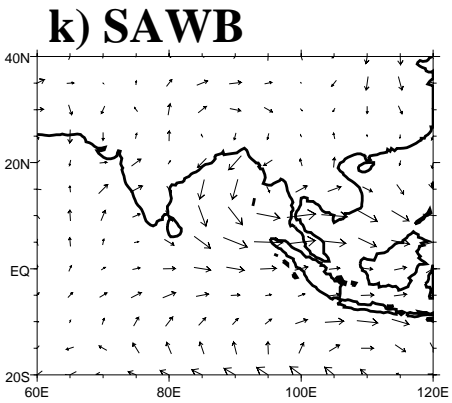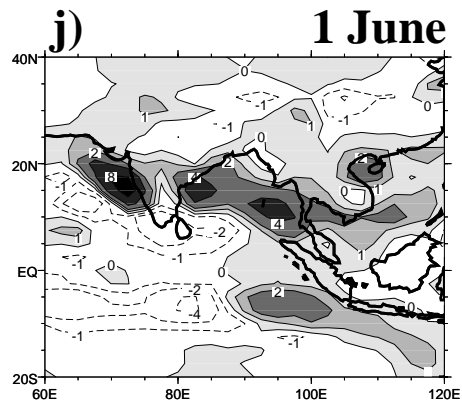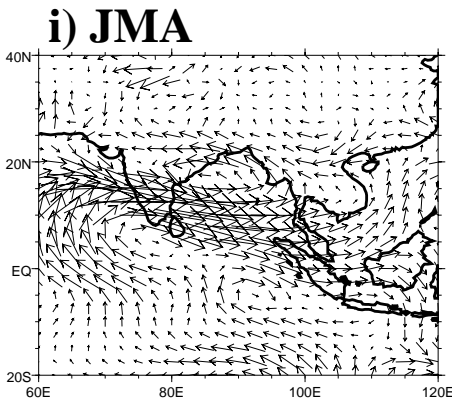
Figure 14: As Fig. 13, but for ensemble members in 1993 that had the correct signs of the projections of at least the first two principal component timeseries.

-46-

850hPa winds

i) JMA

k) SAWB

m) UKMO

2.5

Rainfall

j)   1 June

l)   30 May

n)   28, 30, 31 May

Figure 14 (con't)

hanced rainfall over India due to the incorrect rainfall pattern associated with this mode (Fig. 6g) as discussed in Section 5c. But, this error is minimized due to the relatively small loading of $\overline{PC\text{-}1}$ for this member. As seen in Fig. 13g this member is more realistic in representing the onshore flow along the west coast of India than the average over all members (Fig. 11m). With this improved flow there is enhanced rainfall there (Fig. 13h). However, southeasterly anomalies along the monsoon trough are still absent due to the weak projection of $\overline{PC\text{-}3}$, and the enhanced rainfall over northeastern India is still underestimated.

The 31 May 1988 UKMO simulation shows the most substantial improvement given the correct loading of $\overline{PC\text{-}4}$ ($\overline{PC\text{-}3}$ from reanalysis; Table 8). As seen in Fig. 13i, this member has a more realistic orientation of the flow along the monsoon trough and the cyclonic flow southwest of India relative to Fig. 11o. Additionally, the strong cyclonic flow at the head of the Bay of Bengal, previously noted in Fig. 11o, has been reduced and is therefore more realistic in Fig. 13i. Associated with the improved 850hPa wind anomalies is a more realistic representation of the enhanced rainfall anomalies over India and the below-normal anomalies over the Bay of Bengal, as seen in Fig. 13j.

As mentioned in Section 5d, during 1993 virtually all models had at least one member that simulated the correct sign of the observed projections of $\overline{PC\text{-}1}$ and $\overline{PC\text{-}2}$. However, difficulties in simulating the positive projection of $\overline{PC\text{-}3}$ will limit the benefit obtained from correctly representing the signs of $\overline{PC\text{-}1}$ and $\overline{PC\text{-}2}$.

The 29 May 1993 BMRC member anomalies are given in Figs. 14a and b. There is definite improvement with the presence of northwesterly anomalies over northern India. This is however, incorrectly related to the northward displacement of the westerlies in EOF-1 (Fig. 3b) associated with the positive projection of $\overline{PC\text{-}1}$ and the strong negative projection of $\overline{PC\text{-}3}$. The rainfall pattern is also problematic (Fig. 14b), again due to the incorrect sign of the composite rainfall for EOF-1/PC-1 over India (Fig. 6b). This highlights the necessity of accurately simulating the regionality of the subseasonal modes and their relationship with rainfall.

As seen in Fig. 14c, the 29 May 1993 CNRM run exhibits improved northwesterly flow over India and consequently stronger rainfall anomalies over this region (Fig. 14d). The southeasterly anomalies that extend inland from the northwest Bay of Bengal are still poorly represented due to the southward displacement of the 850hPa flow and its associated rainfall for EOF-2/PC-2 (Figs. 4c and 7c). This contributes to the incorrect negative rainfall anomalies over northeast India seen in Figs. 12f and 14d.

The 30 May 1993 DNM integration captures the correct signs of $\overline{PC\text{-}7}$ and $\overline{PC\text{-}4}$ ($\overline{PC\text{-}1}$ and $\overline{PC\text{-}3}$ from reanalysis), favorably exhibiting an increase in the westerlies over northwest India and the Arabian Sea (Fig. 14e). This is associated with positive rainfall anomalies over this region (Fig. 14f), a modest improvement relative to the anomalies based on all members (Fig. 12h).

For ECMWF, the wind and rainfall anomalies from the composite of the 23, 25, 29-31 May (Table 5) integrations do not show any improvement in the 850hPa and the rainfall anomalies (Figs. 14g and h) even though the signs of the projections of the $\overline{PC's}$ agree with the reanalysis (Table 5). Two reasons contribute to this shortfall: (1) as noted earlier the incorrect sign of the $\overline{PC\text{-}1}$ composite rainfall anomalies over India (Fig. 6e) and (2) the stronger contributions of higher order modes (not shown).

JMA shows dramatic improvement in its 1 June 1993 simulation as seen in Figs. 14i and j, especially in light of the positive projection of $\overline{PC\text{-}1}$. However, the excessively strong positive projection of $\overline{PC\text{-}3}$ also contributes to the enhanced rainfall in the vicinity of India, which is stronger than observed.

For SAWB, the 30 May 1993 simulation has the correct sign of the observed projections of $\overline{PC\text{-}1}$ and $\overline{PC\text{-}2}$ (Table 7). As seen in Fig. 14k, the westerly anomalies near the west coast of India are an improvement relative to Fig. 12m mainly due to the relatively stronger projection of $\overline{PC\text{-}1}$ over $\overline{PC\text{-}2}$. As with BMRC and ECMWF, the incorrect rainfall over India associated with EOF-1/PC-1 (Fig. 6g) contributes to the incorrect rainfall anomalies over this region in 1993.

From UKMO the 28, 30 and 31 May 1993 runs correctly simulate the signs of the $\overline{PC\text{-}1}$ and $\overline{PC\text{-}2}$. The composite northwesterly anomalies over India and the Bay of Bengal (Fig. 14m) are stronger relative to the anomalies based on all members of the 1993 ensemble (Fig. 12o). These anomalies are associated with an improvement of the rainfall anomalies (Fig. 14n) over northwest India and around the rim of the Bay of Bengal. The improvement is in part accounted for by the overly strong projection of $\overline{PC\text{-}1}$, but the correct sign of $\overline{PC\text{-}2}$ from these members also contribute to the improvement (Table 8).

We have been able to stratify model performance according to the projections of the subseasonal modes onto the interannual variability. In the majority of cases, the 850hPa wind and the rainfall anomalies were improved in those subsets of simulations that correctly simulated the sign of the observed projections, especially for those models that were most realistic at representing the subseasonal link between the 850hPa flow and the rainfall. The improvement is tempered by the need to also sim-

ulate more realistic magnitudes of the observed $\overline{PC's}$, and the basic requirement that the rainfall associated with each of the subseasonal modes be well simulated.

6. Discussion and conclusions

We have investigated dynamical seasonal predictability of the Asian summer monsoon using ensembles of hindcasts from seven models forced with observed SSTs and run from observed initial conditions. DSP is addressed by evaluating the link between subseasonal and interannual variability. With respect to the goals of the paper outlined in Section 1, firstly, our results indicate that a high degree of fidelity is required in the simulation of the dominant modes of subseasonal variability. Errors in the spatial patterns of the modes relative to observations inhibit the simulation of the observed interannual anomalies, and are related to errors in the mean state of the model.

Secondly, the rainfall anomalies associated with the subseasonal modes must agree well with the observations in order to have the potential for DSP of rainfall. Errors in the magnitude and spatial patterns of the subseasonal rainfall anomalies are detrimental to DSP since they can result in the incorrect sign of the anomalies on interannual timescales, and contribute to errors in the time-mean state of rainfall. In this respect the most dramatic example is the simulation of rainfall anomalies of the incorrect sign over India with respect to EOF-1/PC-1 in the case of BMRC, DNM, EC-MWF and SAWB (Figs. 6b, e, and g). In these cases, even though a model may properly project this mode onto the interannual variability, the rainfall signal over India will be of opposite sign relative to the observed projection. Over and above this, it is readily apparent that even where the sign of the rainfall anomalies agree with observations in Figs. 6-8, the magnitudes can differ substantially making quantitative assessment of the total seasonal anomaly an extremely challenging problem.

Thirdly, the models usually fail to properly project the subseasonal modes onto the seasonal mean monsoon with the result of poor DSP of the Asian summer monsoon. In the cases where the subseasonal modes and their associated rainfall variations are well simulated by a model, and the modes are known to be linked to aspects of the boundary forcing, projections of the incorrect sign indicate that the model is not generating the necessary teleconnections. A prime example is the JMA model, which gives an excellent representation of the subseasonal modes and their associated rainfall patterns (Figs. 3f-8f). In particular, the subseasonal mode that is most important for all-India rainfall is best simulated by this model (EOF-3, Fig. 5f). However, the interannual variability of this mode is incorrectly simulated (Table 6 and Fig. 9n),

contributing directly to the poor simulation of the 850hPa wind and rainfall anomalies over India (and the ASM region in general, Figs. 10k-l and 11k-l). In the case of the El Niño forced mode (EOF-2/PC-2, Sperber et al. 2000) the poor projections by the models could be related to errors in the location, magnitude and vertical representation of the ENSO-related diabatic heating.

Fourthly, we find that given a reasonable representation of the subseasonal modes and their associated rainfall variations it is found that when an ensemble member can at least simulate the correct signs of the observed projections these members give a more realistic representation of the observed anomalies. This serves as a method of objectively discriminating among the ensemble members, although only in an *a posteriori* manner. More accurate DSP would be achieved if more realistic relative loadings of the $\overline{\text{PC's}}$ were captured by the models, but this is presently beyond the scope of the current models used for DSP. Importantly, this study also sheds light on the subseasonal mode or modes that are associated with systematic model error on interannual timescales and in their time-mean states. If the underlying physics of the various subseasonal modes can be understood in detail, this would result in improvement of all aspects of a models variability.

Additionally, the results in Figs. 3-8 indicate that there may be a sensitivity to horizontal resolution. The two coarsest resolution models, DNM and SAWB (Table 1), have difficulty in representing the subseasonal modes, including the strong gradients and regional-scale features in the 850hPa flow. This result is consistent with the horizontal resolution study of Sperber et al. (1994), the only resolution study to examine subseasonal variability of the ASM for the range of resolutions in Table 1. They found that T21 was inadequate for simulating the synoptic-scale evolution of the monsoon trough and variations of the Mei-yu rainband over China. Rather, they determined that horizontal resolution of T106 (~1.125°) was required to simulate these phenomena. Subsequent improvement is suggested by the results presented herein, and the results of Martin (1999) who found that 2.5°x3.75° (~T42) is adequate for the simulation of intraseasonal variability of the summer monsoon. However, these afore-mentioned resolution studies, and those of Tibaldi et al. (1990), Lal et al. (1997) and Stephenson et al. (1998) indicate that increasing horizontal resolution is not the panacea for improving the simulation of summer monsoon variability. Rather, the interaction between physics parameterizations, in particular convection, and resolution (both horizontal and vertical) needs to be understood in more detail.

References

Alekseev V.A., E. M. Volodin, V. Galin, V. P. Dymnikov, and V. N. Lykossov, 1999: Modeling of the present-day climate by the atmospheric model of INM RAS "DNM GCM". Description of the model version A5421 and results of AMIP II simulations. INM report N2086-B98. Institute for Numerical Mathematics, Gubkina 8, Moscow 117951 GSP-1, Russia.

Annamalai, H., J. M. Slingo, K. R. Sperber, and K. Hodges, 1999: The mean evolution and variability of the Asian summer monsoon: comparison of ECMWF and NCEP/NCAR reanalyses. *Mon. Wea. Rev.*, **127**, 1157-1186.

Barnett, T. P., L. Dumenil, U. Schlese, E. Roeckner, and M. Latif, 1989: The effect of Eurasian snow cover on regional and global climate variations. *J. Atmos. Sci.*, **46**, 661-685.

Becker, B. D., J. M. Slingo, L. Ferranti, and F. Molteni, 2000: Seasonal predictability of the Indian summer monsoon: What role do land surface conditions play? *Mausam*, (in press).

Blanford, H. F., 1884: On the connection of the Himalaya snowfall with dry winds and seasons of drought in India. *Proc. Roy. Soc.*, **37**, 3-22.

Branković, C. and T. N. Palmer, 2000: Seasonal skill and predictability of ECMWF PROVOST ensembles. *Q. J. Roy. Meteorol. Soc.* (in press).

Charney, J. G. and J. Shukla, 1981: Predictability of monsoons. Chapter in "Monsoon Dynamics", Cambridge University Press, pp. 99-110.

Déqué M. and J. P. Piedelievre, 1995: High resolution climate simulation over Europe. *Clim. Dynam.*, **11**, 321-339.

Fennessy, M. J. and J. Shukla, 1994: GCM simulations of active and break monsoon periods. Proc. of the International Conference on Monsoon Variability and Prediction, Trieste, Italy, WCRP-84, WMO/TD-No. 619, Vol. 2, 576-585.

Ferranti, L. and F. Molteni, 1999: Ensemble simulations of Eurasian snow-depth anomalies their influence on the summer Asian monsoon. *Quart. J. Roy. Meteorol. Soc.*, **125**, 2597-2610.

Ferranti, L., J. M. Slingo, T. N. Palmer, and B. J. Hoskins, 1997: Relations between interannual and intraseasonal monsoon variability as diagnosed from AMIP integrations. *Q. J. Roy. Meteorol. Soc.*, **123**, 1323-1357.

Gadgil, S. and G. Asha, 1992: Intraseasonal variation of the summer monsoon I: observational aspects. *J. Meteorol. Soc. Japan*, **70**, 517-527.

Gibson, J. K., P. Kallberg and S. Uppala, 1996: The ECMWF ReAnalysis (ERA) project. ECMWF Newsletter No. 73, ECMWF, Shinfield Park, Reading, UK.

Gibson, J. K., P. Kallberg, S. Uppala, A Hernandez, A. Nomura, and E. Serano, 1997: ECMWF ReAnalysis Project Rep. Series 1, ECMWF, Shinfield Park, Reading, UK. 72pp.

Graham, R. J., A. D. L. Evans, K. R. Mylne, M. S. J. Harrison, K. B. Robertson, 2000: An assessment of seasonal predictability using Atmospheric General Circulation Models. *Q. J. Roy. Meteorol. Soc.* (submitted).

Hall, C. D., R. A. Stratton and M. L. Gallani, 1995: Climate simulations with the Unified Model: AMIP runs. UK Meteorological Office Climate Research Technical Note 61. Available from the National Meteorological Library, London Road, Bracknell, Berkshire, RG12 2SZ, UK.

Hart, T.L., W. Bourke, B. J. McAvaney, B. W. Forgan, and J. L. McGregor, 1990: Atmospheric general circulation simulations with the BMRC global spectral model: the impact of revised physical parameterizations. *J. Clim.*, **3**, 436-459.

JMA, 1997: Outline of operational numerical weather prediction at the Japan Meteorological Agency. Numerical Prediction Division, Japan Meteorological Agency, Tokyo.

Kalnay, E., M. Kanamitsu, R. Kistler, W. Collins, D. Deaven, L. Gandin, M. Iredell, S. Saha, G. White, J. Woollen, Y. Zhu, M. Chelliah, W. Ebisuzaki, W. Higgins, J. Janowiak, K.C. Mo, C. Ropelewski, J. Wang, A. Leetma, R. Reynolds, R. Jenne and D. Joseph, 1996: The NCEP/NCAR 40-year reanalysis project. *Bull. Amer. Met. Soc.*, **77**, 437-471.

Kirtman, B.P., J. Shukla, B. Huang, Z. Zhu and E.K. Schneider, 1997; Multiseasonal predictions with a coupled tropical ocean-global atmosphere system. *Mon. Wea. Rev.*, **125**, 789 - 808.

Krishna Kumar, K., M. K. Soman, and K. Rupa Kumar, 1995: Seasonal forecasting of Indian summer monsoon rainfall. *Weather*, **50**, 449-467.

Krishnamurti, T. N. and H. N. Bhalme, 1976: Oscillations of the monsoon system. part 1. observational aspects. *J. Atmos. Sci.*, **33**, 1937-1954.

Lal, M, U. Cubasch, J, Perlwitz, and J. Waszkewitz, 1997: Simulation of the Indian monsoon climatology in ECHAM3 climate model: sensitivity to horizontal resolution. *Int. J. Climatol.*, **17**, 847-858.

Martin, G., 1999: The simulation of the Asian summer monsoon, and its sensitivity to horizontal resolution, in the UK Meteorological Office Unified Model. *Q. J. Roy. Meteorol. Soc.*, **125**, 1499-1525.

McAvaney, B. J. and R. A. Colman, 1993: The AMIP experiment: The BMRC AGCM Configuration, BMRC Research Report, 38, 43pp. Bureau of Meteorology.

Miller, M., M. Hortal, and C. Jakob,1995: A major operational forecast model change. *ECMWF Newsletter*, **70**, 2-5.

Mo, K. C. and R. W. Higgins, 1996: Large-scale atmospheric moisture transport as evaluated in the NCEP/NCAR and the NASA/DAO reanalyses. *J. Clim.*, **9**, 1531-1545.

Normand, C., 1953: Monsoon seasonal forecasting. *Q. J. Roy. Meteorol. Soc.*, **79**, 463-473.

Palmer, T. N.,1994: Chaos and predictability in forecasting the monsoon. *Proc. Indian Nat. Sci. Acad.*, **60A**, 57-66.

Pan, H. L. and L. Mahrt, 1987: Interaction between soil hydrology and boundary layer developments. *Bound. Layer Met.*, **38**, 185-202.

Pan, H. L. and W. S. Wu, 1994: Implementing a mass-flux convection parameterization package for the NMC medium-range forecast model. Proceedings of the Tenth Conference on Numerical Weather Prediction, Portland/Oregon, pp. 96-98.

Sikka, D. R. 1980: Some aspects of the large-scale fluctuations of summer monsoon rainfall over India in relation to fluctuations in the planetary and regional scale circulation parameters. Proceedings of the Indian Academy of Science (*Earth and Planet. Sci.*), **89**, 179-195.

Slingo, J. M. 1987: The development and verification of a cloud prediction scheme for the ECMWF model. *Q. J. Roy. Meteorol. Soc.*, **113**, 899-927.

Sperber, K. R., S. Hameed, G. L. Potter, and J. S. Boyle, 1994: Simulation of the northern summer monsoon in the ECMWF model: sensitivity to horizontal resolution. *Mon. Wea. Rev.*, **122**, 2461-2481.

Sperber, K. R. and T. N. Palmer, 1996: Interannual tropical rainfall variability in general circulation model simulations associated with the Atmospheric Model Intercomparison Project. *J. Clim.*, **9**, 2727-2750.

Sperber, K. R., J. M. Slingo, and H. Annamalai,1999: Predictability and the relationship between subseasonal and interannual variability during the Asian summer monsoon. PCMDI Report No. 53. Lawrence Livermore National Laboratory, P.O. Box 808, L-264, Livermore, CA 94550. (http://www-pcmdi.llnl.gov/pcmdi/pubs/ab53.html), 53pp.

Sperber, K. R., J. M. Slingo, and H. Annamalai, 2000: Predictability and the relationship between subseasonal and interannual variability during the Asian summer monsoon. *Q. J. Roy. Meteorol. Soc.*, (in press)

Stendel, M. and K. Arpe, 1997: Evaluation of the hydrological cycle in reanalyses and observations. Report No. 228, Max-Planck-Institut für Meteorologie, Hamburg, Germany.

Stephenson, D. B., F. Chauvin, and J.-F. Royer, 1998: Simulation of the Asian summer monsoon and its dependence on model horizontal resolution. *J. Meteorol. Soc. Japan*, **76**, 237-265.

Tennant, W.J., 1999: The potential for the numerical forecasting of monthly climate over South Africa. *Int. J. Climatol.*, **19**, 1319 - 1336.

Tibaldi, S., T. N. Palmer, C. Brankovic, and U. Cubasch, 1990: Extended-range predictions with ECMWF models: influence of horizontal resolution on systematic error and forecast skill. *Q. J. Roy. Meteorol. Soc.*, **116**, 835-866.

Tiedtke, M., 1989: A comprehensive mass flux scheme for cumulus parametrisation. *Mon. Wea. Rev.*, **117**, 1779-1800.

Tiedtke, M., 1993: Representation of clouds in large-scale models, *Mon. Wea. Rev.,* **121**, 3040-3061.

Viterbo, P. and A. C. M. Beljaars, 1995: An improved land surface parametrization scheme in the ECMWF model and its validation. *J. Clim.,* **8**, 2716-2748.

Walker, G. T. and E. W. Bliss, 1930: Some applications to seasonal foreshadowing. *Mem. Roy. Meteorol. Soc.*, **3**, 81-95.

Webster, P. J. and S. Yang, 1992: Monsoon and ENSO: Selectively interactive systems *Q. J. Roy. Meteorol. Soc.*, **118**, pp. 877-926.

Webster, P. J., T. N. Palmer, M. Yanai, J. Shukla, V. Magnana, T. Yasunari and R. Tomas, 1998: The Monsoon: Processes, predictability and prediction. *J. Geophys. Res.*, **103**, 14,451-14510.

Xie, P. and P. Arkin, 1996: Analyses of global monthly precipitation using gauge observations, satellite estimates and numerical model predictions. *J. Clim.*, **9**, 840-858.

Xie, P. and Arkin, P. 1997: Global precipitation: A 17-year monthly analysis based on gauge observations, satellite estimates, and numerical model outputs. *Bull. Amer. Meteorol. Soc.*, **78**, 2539-2558.